https://doi.org/10.5194/egusphere-2026-1868
Preprint. Discussion started: 29 May 2026

Comprehensive Treatment of C_4-C_6 Alkanes and Their Oxidation Products in CAM-chem: The MOZART-T3 Mechanism

Duseong S. Jo[1*], John J. Orlando[2], Rebecca H. Schwantes[3], Louisa K. Emmons[2], Rebecca S. Hornbrook[2], Eric C. Apel[2], Alan J. Hills[2], Kirk Ullmann[2], L. Gregory Huey[4], Claire Granier[3,5,6], Chelsea R. Thompson[3], and Jeff Peischl[3]

[1]Department of Earth Science Education, Seoul National University, Seoul, 08826, South Korea
[2]Atmospheric Chemistry Observations & Modeling Laboratory, NSF National Center for Atmospheric Research, Boulder, CO, 80301, USA
[3]Chemical Sciences Laboratory, National Oceanic and Atmospheric Administration, Boulder, CO, 80305, USA
[4]School of Earth and Atmospheric Sciences, Georgia Institute of Technology, Atlanta, GA, 30332, USA
[5]Laboratoire d'Aerologie, University of Toulouse, CNRS, UPS, Toulouse, France
[6]Cooperative Institute for Research in Environmental Sciences (CIRES), University of Colorado, Boulder, CO 80309, USA

Correspondence to: Duseong S. Jo (duseong@snu.ac.kr)

Abstract. Most global atmospheric chemistry models represent ≥C_4 alkanes using lumped surrogates, limiting both detailed simulation of their oxygenated products and evaluation against comprehensive observational datasets. We present MOZART-T3, which replaces the lumped BIGALK representation with a more explicit treatment of individual C_4–C_6 alkane species and resolves propane peroxy radical isomers, enabling more mechanistically consistent alkane chemistry in the Community Atmosphere Model with chemistry (CAM-chem). Global simulations demonstrate that T3 maintains similar total alkane burdens compared to previous mechanisms, while substantially altering oxygenated product budgets and distributions. Relative to MOZART-T1, T3 significantly reduces the global burden of methyl ethyl ketone (MEK) primarily through incorporation of more comprehensive n-butane oxidation chemistry, with additional contributions from increased photolysis rates and updated emission speciation. T3 introduces six additional C_5–C_6 ketone species that contribute ~40% to global ketone sources but only ~2% to the total burden due to their short lifetimes. The acetaldehyde burden decreases by 8–14% through compound-specific yields that replace the fixed yield in previous mechanisms. The choice of anthropogenic emission inventory drives larger variations in alkane burdens (~24%) than does mechanism complexity (~4%), but mechanism choice dominates for oxidation products. T3 enables evaluation of previously unrepresented species including individual alkanes, propanal, and peroxypropionyl nitrate, with generally improved simulation of oxygenated compounds, although the evaluation results vary temporally and spatially. While lumped approaches sufficiently represent global-scale major pollutant concentrations, T3's detailed treatment enables more comprehensive evaluation and is expected to be more important for urban air quality applications using higher-resolution regional simulations.

https://doi.org/10.5194/egusphere-2026-1868
Preprint. Discussion started: 29 May 2026

1 Introduction

Atmospheric chemical mechanisms serve as the fundamental core of atmospheric chemistry models (Kaduwela et al., 2015), providing the essential framework for both box and three-dimensional models. These mechanisms form the basis for most atmospheric chemistry research applications, including air quality forecasting, climate change predictions, top-down emission estimates, and calculations of trace gas and aerosol lifetimes. Consequently, the accuracy of chemical mechanisms is crucial not only for specialized atmospheric chemistry models but also for comprehensive Earth system models that integrate atmospheric composition with climate and biogeochemical cycles.

Previous studies have shown that the choice of chemical mechanisms can lead to different concentrations of gases and aerosols (Bates and Jacob, 2019; Schwantes et al., 2020; Lin et al., 2024). However, there cannot be a perfect chemical mechanism because the atmosphere contains millions of species and reactions (Goldstein and Galbally, 2007; Ervens et al., 2024). Most of these species and reactions are not directly measured but are instead predicted by automated chemical mechanisms using structure-activity relationships (SARs) (Aumont et al., 2005; Mouchel-Vallon et al., 2020). Therefore, atmospheric models typically simulate only representative species and use simplification approaches such as lumping minor species together to make the mechanisms computationally feasible.

The complexity of chemical mechanisms varies dramatically depending on the research purpose and application. For example, the Master Chemical Mechanism (MCM) v3.3.1, designed for detailed atmospheric chemistry studies in 0D box models, contains 5,832 species and 17,224 reactions (Jenkin et al., 2015). In contrast, 3D atmospheric models require more simplified approaches: GEOS-Chem version 14.1.1 uses 286 species and 914 reactions (Lin et al., 2024), while the Community Regional Atmospheric Chemistry Multiphase Mechanism (CRACMM) v1.0 includes 229 species and 508 reactions (Pye et al., 2023). At the most simplified end, climate models such as the Community Atmosphere Model (CAM) version 6 use only 25 species and 7 reactions for aerosol simulations (Jo et al., 2023a). This variation reflects the fundamental trade-off between chemical fidelity and computational feasibility that governs atmospheric chemistry modeling.

While detailed chemistry with more compounds does not necessarily guarantee better model performance, it provides valuable insights into atmospheric processes and enables comprehensive evaluation of chemical reaction sets. Recent advances in measurement techniques have made more chemical species available from observations (Thompson et al., 2022; Asher et al., 2025), offering additional tracers for model evaluation when these species are included in the mechanisms. These species include both volatile organic compounds (VOCs) and oxygenated VOCs, particularly alkane and alkane-derived species such as isobutane, organic nitrates, and methyl ethyl ketone (MEK), which provide critical constraints on alkane oxidation pathways.

Traditionally, $\geq C_4$ alkanes and their oxidation products have been lumped together for computational efficiency in widely used mechanisms, including the Model for Ozone and Related chemical Tracers (MOZART) series (Brasseur et al., 1998; Emmons et al., 2020) and GEOS-Chem mechanisms (Bey et al., 2001; Tzompa-Sosa et al., 2019). While this lumping approach is computationally efficient, it cannot distinguish several major VOCs and OVOCs in the atmosphere. Additionally, the implicit treatment of major OVOC formation limits accurate simulation and evaluation of alkane oxidation pathways

https://doi.org/10.5194/egusphere-2026-1868
Preprint. Discussion started: 29 May 2026

against increasingly available observations. For example, MEK in MOZART-T1 and GEOS-Chem mechanisms is formed through reactions of NO with peroxy radicals from lumped ≥C_4 alkanes with a fixed yield. Consequently, the MEK tracer in these mechanisms represents not only MEK itself but also implicitly includes higher ketones such as pentanones. Furthermore, lumping of ≥C_4 alkanes can lead to underestimation of OH reactivity (Kim et al., 2022). To address this issue, a recent study by Travis et al. (2024) introduced a new lumped species in GEOS-Chem for ≥C_6 alkanes (ALK6) while maintaining ALK4 for lumped butanes and pentanes.

In this study, we extend the MOZART chemical mechanisms to include detailed alkane chemistry by considering isomers of propane oxidation products and expanding the single surrogate compound (BIGALK) for ≥C_4 alkanes and their oxidation products. We refer to this enhanced mechanism as MOZART-T3. The newly added species include four additional explicit alkane species (two for butanes and two for pentanes) and various OVOCs derived from alkanes, such as peroxy propionyl nitrate (PPN), butanal, and 2- and 3-pentanone. Section 2 describes the updates to the existing mechanism, including newly added species, kinetic and photolysis reactions, emissions, and parameters such as effective Henry's law constants. Section 3 describes the model simulation setup, including emissions, meteorology, and simulation periods. Section 4 presents a comparison of simulations using MOZART-T1, MOZART-T2, and MOZART-T3 mechanisms in terms of global features including burden, vertical profiles, and lifetimes. Additionally, we employ two different anthropogenic emission inventories to compare the effects of emission differences versus chemical mechanism differences on various chemical species. Section 5 provides model evaluation results against the NASA Atmospheric Tomography (ATom) global aircraft campaign (Thompson et al., 2022), to globally assess the relative importance of chemical mechanism updates versus emission inventory changes in model performance.

https://doi.org/10.5194/egusphere-2026-1868
Preprint. Discussion started: 29 May 2026

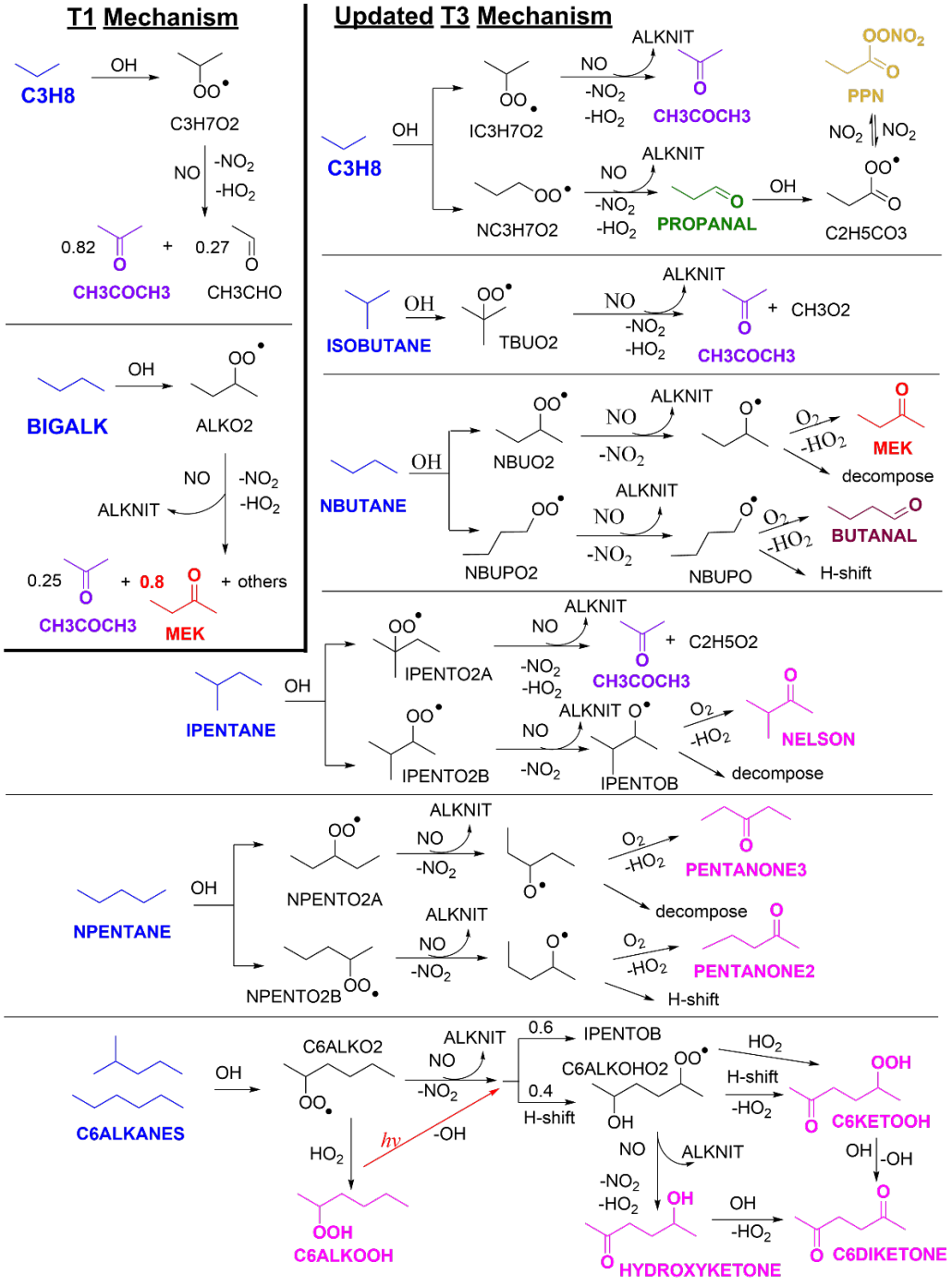

Figure 1. Simplified comparison of alkane oxidation schemes in MOZART-T1 versus MOZART-T3 mechanisms. Reaction pathways show RO_2 + NO chemistry with branching ratios where applicable. C6ALKANES pathway illustrates the complete oxidation scheme including RO_2 + NO, RO_2 + HO_2 reactions, and hydrogen shift reactions. MOZART-T2 chemistry is identical to T1 for alkanes.

https://doi.org/10.5194/egusphere-2026-1868
Preprint. Discussion started: 29 May 2026

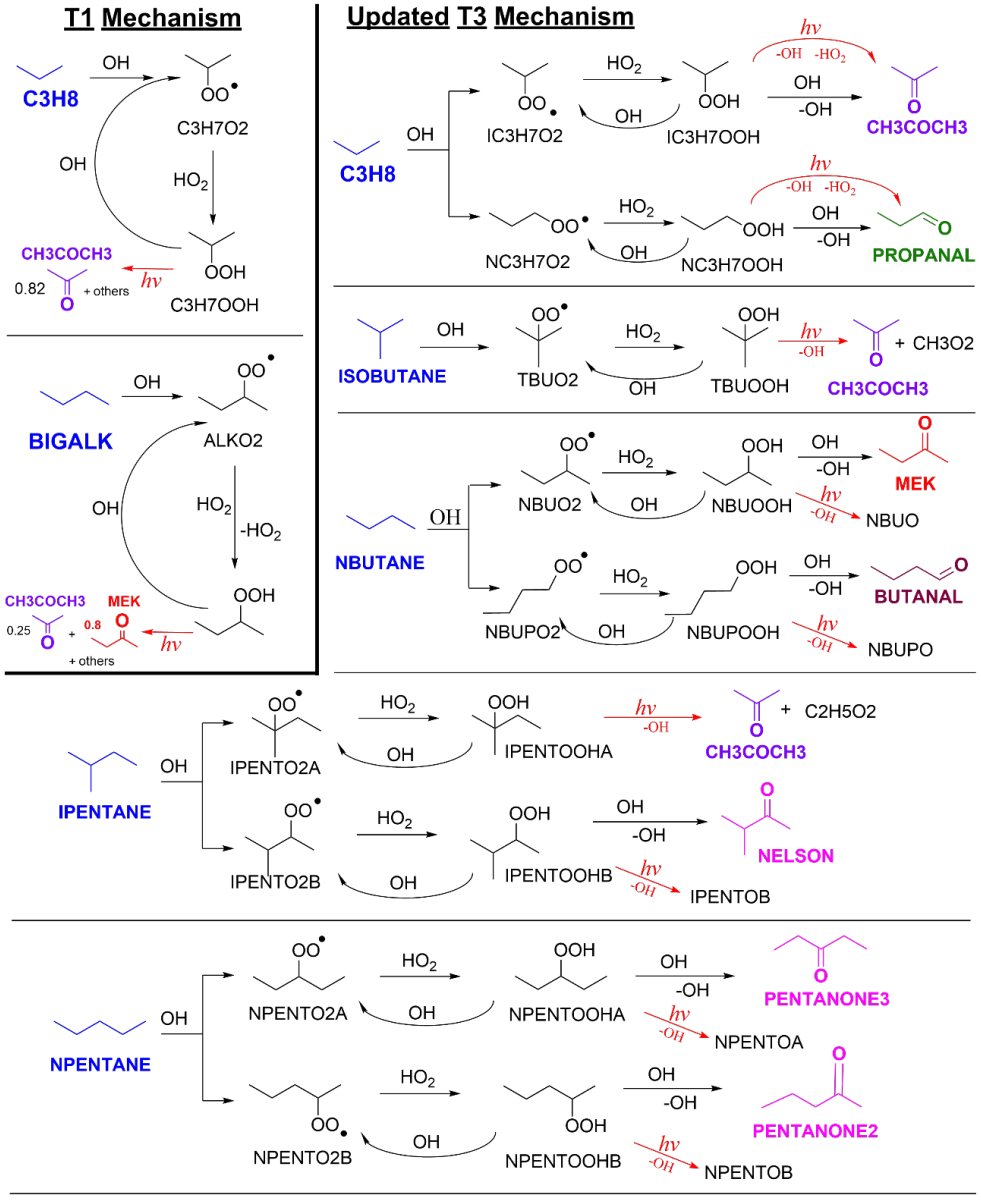

Figure 2. Simplified comparison of alkane oxidation schemes in MOZART-T1 versus MOZART-T3 mechanisms. Reaction pathways show $RO_2 + HO_2$ chemistry with branching ratios where applicable. C6ALKANES pathway is shown in Fig. 1. MOZART-T2 chemistry is identical to T1 for alkanes.

https://doi.org/10.5194/egusphere-2026-1868
Preprint. Discussion started: 29 May 2026

2 Chemical Mechanism Development

Previous versions of the MOZART mechanism, including MOZART-T1 (Emmons et al., 2020 , hereafter "T1") and MOZART-T2 (Schwantes et al., 2020 , hereafter "T2"), represent all ≥C_4 alkanes using a single surrogate compound (BIGALK). In contrast, MOZART-T3 (hereafter "T3"), developed in this work, explicitly resolves five alkane species: n-butane (NBUTANE), i-butane (ISOBUTANE), n-pentane (NPENTANE), i-pentane (IPENTANE), and C≥6 alkanes (C6ALKANES), as illustrated in Figs. 1 and 2. Additionally, T3 includes more detailed propane (C3H8) chemistry with explicit simulation of propyl peroxy radical isomers (Figs. 1 and 2). Complete descriptions of all T3 kinetic reactions (Table S1), photolysis reactions (Table S2), species list (Table S3), and parameters (effective Henry's law constants and reactivity factors) for dry and wet deposition (Table S4) are provided in the Supplement.

2.1 Main sources used for T3 mechanism

The development of T3 is guided by comprehensive reviews of alkane chemistry (Atkinson and Arey, 2003; Orlando et al., 2003; Atkinson, 2007; Calvert et al., 2008, 2011, 2015; Dibble and Chai, 2017) and explicit mechanisms such as MCM v3.3.1 (Jenkin et al., 1997; Saunders et al., 2003). Reaction rate constants are primarily taken from IUPAC recommendations (Atkinson et al., 2004, 2006) and JPL Publication 19 (Burkholder et al., 2019). For reactions lacking experimental rate data, we employ SARs following the methodologies established by Jenkin et al. (2018, 2019), Vereecken and Peeters (2009), and Vereecken and Nozière (2020), analogous to the treatment in MCM v3.3.1.

2.2 The initial reactions of alkanes with OH

All alkanes are oxidized through bimolecular reaction with OH followed by O_2 addition to form alkyl peroxy radicals. For propane (C3H8) and n-butane (NBUTANE), we explicitly simulate the hydrogen abstraction site based on the temperature-dependent primary to secondary branching ratios reported by Droege and Tully (1986). We apply these ratios to the total reaction rates recommended by IUPAC for the 200–330 K temperature range and fit the resulting site-specific rates to Arrhenius expressions. The derived Arrhenius equations accurately reproduce the temperature dependence of both primary and secondary peroxy radical formation, with r^2 of 0.998 and a regression slope of 0.996. For i-butane (ISOBUTANE), we neglect primary peroxy radicals for computational efficiency, as the tertiary channel is dominant. For pentanes (NPENTANE and IPENTANE), we use branching ratios from Calvert et al. (2015), again neglecting primary peroxy radicals to reduce computational cost. For ≥C_6 alkanes (C6ALKANES), we use a single reaction rate averaged from the ≥C_6 alkane rates reported in Calvert et al. (2015).

2.3 The reactions of peroxy radicals with NO, HO_2, and NO_3

The reaction of alkyl peroxy radicals with NO proceeds through two competing channels: (1) formation of alkoxy radicals with NO-to-NO_2 conversion, and (2) formation of organic nitrates. To account for the temperature and pressure

https://doi.org/10.5194/egusphere-2026-1868
Preprint. Discussion started: 29 May 2026

dependence of organic nitrate formation (with higher yields at lower temperatures), we employ the branching ratio parameterization from Jenkin et al. (2019). This method produces results consistent with the carbon-number-dependent formula from Arey et al. (2001) at 298 K and 740 Torr. For example, the organic nitrate yields for C_2–C_6 alkanes in this study are 0.022, 0.041, 0.067, 0.105, and 0.162, respectively, compared to 0.003, 0.041, 0.079, 0.118, and 0.156 from Arey et al. (2001).

We do not apply additional adjustments based on peroxy radical structure (i.e., primary, secondary, or tertiary) due to unresolved uncertainties. As detailed by Orlando and Tyndall (2012) and Wennberg et al. (2018), significant disagreement exists among past studies regarding the influence of molecular structure on organic nitrate yields, warranting further experimental investigation. In T3, all alkane-derived organic nitrates are represented by a single surrogate species (ALKNIT), parameterized to behave like a pentyl nitrate. This choice reflects the dominance of C_4–C_6 alkyl nitrates in the global budget due to their higher yields from longer-chain alkanes (Arey et al., 2001; Jenkin et al., 2019). For example, using CEDS emissions with T3 organic nitrate yields, global ALKNIT production in 2016–2018 consists of contributions from C_2 (9%), C_3 (8%), C_4 (12%), C_5 (17%), and C_6 (54%) alkyl peroxy radicals (Sect. 4).

Reaction rates of alkyl peroxy radicals with NO are assumed constant for all $\geq C_3$ species, as experimental data show no significant dependence on peroxy radical identity or structure (Jenkin et al., 2019). Ethyl peroxy radical uses a slightly different rate constant from JPL recommendations, following the T1 mechanism.

For non-acyl peroxy radical reactions with HO_2, only the hydroperoxide formation pathway is considered (Fig. 2), as it dominates under atmospheric conditions. Rate constants are calculated using the parameterization recommended by Wennberg et al. (2018), derived from the sum of carbon, oxygen, and nitrogen atoms (excluding peroxy radical oxygen atoms). For acyl peroxy radicals (acetyl and propionyl peroxy), we use temperature-dependent rate constants from IUPAC for three product channels including ozone formation and OH production. Note that T1 and T2 treat these channels without temperature dependency (i.e., fixed branching ratios; see Table S6 in Schwantes et al., 2020).

Peroxy radical reactions with NO_3 are also included, producing alkoxy radicals and NO_2 as in the first channel of RO_2 + NO (alkoxy radical formation), with O_2 as an additional product. Following Jenkin et al. (2019), the same temperature-dependent rate constant is applied for all $\geq C_2$ non-acyl peroxy radicals, yielding 2.4×10^{-12} cm^3 $molecule^{-1}$ s^{-1} at 298 K, comparable to the IUPAC recommendation of 2.3×10^{-12} cm^3 $molecule^{-1}$ s^{-1}.

2.4 The permutation reactions of peroxy radicals

Given the computational cost of explicitly treating all possible RO_2 self- and cross-reactions, we approximate these reactions by considering only the reactions of alkyl peroxy radicals with methyl peroxy radical (CH_3O_2) and acetyl peroxy radical ($CH_3C(O)O_2$). For reactions with CH_3O_2, the radical channel accounts for 60% of primary and secondary peroxy radicals, and 80% for tertiary peroxy radicals, following Jenkin et al. (2019). Reaction rate constants are calculated from the self-reaction rates of each peroxy radical and CH_3O_2, combined with additional scaling factors from Jenkin et al. (2019). One exception is the reaction of tertiary butyl peroxy radical (TBUO2) with CH_3O_2, which uses the IUPAC-recommended rate

https://doi.org/10.5194/egusphere-2026-1868
Preprint. Discussion started: 29 May 2026

constant based on laboratory measurements. For reactions with $CH_3C(O)O_2$, we apply the rate constant of $C_2H_5O_2$ + $CH_3C(O)O_2$ to all $\geq C_3$ alkyl peroxy radicals. The $CH_3C(O)O$ radical is not explicitly simulated, as it undergoes rapid thermal decomposition to form CH_3O_2 and CO_2 (Roehl et al., 1996).

2.5 Alkoxy radical pathways (reaction with O_2, H-shift, and decomposition)

All tertiary alkoxy radicals are assumed to decompose instantaneously. Primary and secondary alkoxy radicals react with O_2 using a generic rate constant of 2.5×10^{-14} exp(-300/T) cm^3 $molecule^{-1}$ s^{-1} estimated by Atkinson (2007). For $\leq C_3$ alkoxy radicals, explicit simulation is omitted for computational efficiency, as their H-shift and decomposition rates are negligibly slow (Atkinson, 2007). Therefore, only the final products from alkane alkoxy radical reactions with O_2 are considered (HO_2 and carbonyl species). Decomposition rate constants for primary and secondary alkane-derived alkoxy radicals are estimated using SARs from Vereecken and Peeters (2009), based on decomposition barrier heights derived from quantum chemical calculations. H-shift rates are estimated using SARs from Atkinson (2007). This treatment is consistent with the approach used in the Generator of Explicit Chemistry and Kinetics for Organics in the Atmosphere (GECKO-A) (Aumont et al., 2005).

Recent work has demonstrated that peroxy radical H-shifts in n-hexane oxidation can compete with bimolecular reactions with NO under ambient atmospheric conditions (Praske et al., 2018). Although much remains unknown about these peroxy radical H-shifts and their applicability to longer-chain alkanes, they are likely particularly important in the remote atmosphere, which is the focus of this work. In T3, as shown in Fig. 1, C6ALKOHO2 (an oxidation product from OH reaction with C6ALKANES) undergoes peroxy radical H-shift to form a hydroperoxy ketone. The temperature-dependent rate constant is taken from measurements for 2-hydroxy-5-peroxy hexane reported by Praske et al. (2018). We note that this rate constant has large uncertainties (within a factor of 10), and its extrapolation to all $\geq C_6$ alkanes represented by the C6ALKANES surrogate is even more uncertain due to limited experimental data and incomplete characterization of $\geq C_6$ alkane composition in emission inventories. However, we include this reaction to evaluate its atmospheric importance (Sect. 4). As more data become available, this reaction parameterization should be refined in future versions of T3.

2.6 Lumped species for C_6 or higher alkanes

The C6ALKANES surrogate represents all $\geq C_6$ alkanes in the mechanism, including their initial OH oxidation and subsequent peroxy radical (C6ALKO2) reactions with HO_2 and NO. To account for alkoxy radical H-shift reactions, we introduce an additional species (C6ALKOHO2), a hydroperoxy alkyl peroxy radical formed from H-shift of the alkoxy radical. Based on measured hydrocarbon ratios (Apel et al., 2010; Swarthout et al., 2013) and considering that some multigenerational products (e.g., from methylcyclopentane) can undergo H-shift, we assume 60% of $\geq C_6$ alkoxy radicals can undergo H-shift to form C6ALKOHO2 (in competition with NO and HO_2 reactions), while 40% do not.

https://doi.org/10.5194/egusphere-2026-1868
Preprint. Discussion started: 29 May 2026

Alkoxy radicals that do not undergo H-shift are lumped with the 3-methyl-2-butoxy radical (IPENTOB) from i-pentane (IPENTANE) oxidation for computational efficiency. C6ALKOHO2 reacts with HO_2 and NO following standard peroxy radical chemistry, and additionally undergoes peroxy radical H-shift based on Vereecken and Nozière (2020), as discussed in Sect. 2.5. Hydroperoxides from both C6ALKO2 and C6ALKOHO2 are combined into a single surrogate species (C6ALKOOH). Both C6ALKOOH and C6KETOOH (the hydroperoxy ketone from C6ALKOHO2 H-shift) undergo OH-initiated reactions leading to either peroxy radical regeneration or carbonyl formation. As with other ketones in the mechanism (e.g., NELSON, PENTANONE2, etc.), further reaction chains from ketone + OH are treated implicitly, generating decomposed products that are already represented in the mechanism.

2.7 Photolysis

Photolysis reactions are added to T3 for some newly introduced species, including hydroperoxides, aldehydes, ketones, and peroxy propionyl nitrate (PPN). For hydroperoxides, we apply the photolysis rate of methyl hydroperoxide (CH3OOH) to all alkane hydroperoxides, as experimental data for $\geq C_2$ hydroperoxides are not available. For PPN, we use the photolysis rate of PAN, as both compounds have similar absorption cross sections and quantum yields (Burkholder et al., 2019).

For $\geq C_3$ aldehydes, we apply a uniform photolysis rate that is twice that of acetaldehyde, based on quantum yield differences between acetaldehyde and propanal (which have similar absorption cross sections) (Horowitz and Calvert, 1982; Atkinson and Lloyd, 1984; Heicklen et al., 1986; Chen and Zhu, 2001; Barnes and Rudzinski, 2006; Burkholder et al., 2019). This is consistent with photolysis rates calculated by the Tropospheric Ultraviolet and Visible (TUV) radiation model (Madronich and Flocke, 1999; Kinnison et al., 2007). In T1 and T2, MEK photolysis was assumed equal to that of acetone, but we have updated it to be five times that of acetone in T3, as discussed in Sect. 2.8. For C≥5 ketones, we assume the same photolysis rate as methyl ethyl ketone (MEK).

2.8 Updates for T1 and T2 mechanisms

The T1 mechanism has undergone several updates since its original publication (Emmons et al., 2020). In this study, we refer to the version prior to this work as T1.2, which includes NO_x-dependent SOA yield parameterization (Jo et al., 2021; Schwantes et al., 2022) and reaction rate constants updated based on JPL Publication 19 (Burkholder et al., 2019). The version incorporating the additional updates described in this section is referred to as T1.3, which serves as the basis for all updated T1- and T2-based simulations in this study (Table 1).

Several kinetic and photolysis reactions common to all mechanisms (T1, T2, and T3) have been updated in T1.3 relative to T1.2, as listed in Table S5. Key updates include: reactions of $\leq C_2$ peroxy radicals (CH_3O_2, $C_2H_5O_2$, CH_3CO_3) with NO_3 added for consistency with T3 chemistry; the reaction rate constant for ALKNIT + OH updated from 1.6×10^{-12} cm^3 $molecule^{-1}$ s^{-1} to 2.2×10^{-12} cm^3 $molecule^{-1}$ s^{-1} based on the average of seventeen C_4–C_8 alkyl nitrate rate constants from Calvert

https://doi.org/10.5194/egusphere-2026-1868
Preprint. Discussion started: 29 May 2026

et al. (2011); and reaction rate constants for $C_3H_7O_2$ with NO, HO_2, and CH_3O_2 in T1 and T2, which were based on Brasseur et al. (1998), have also been updated, based on IUPAC, Jenkin et al. (2019), and Wennberg et al. (2018).

The photolysis rate of MEK has been updated based on recent evidence showing MEK photolyzes faster than acetone. This difference is attributed to quantum yield variations between the two compounds (Raber and Moortgat, 1987; Atkinson et al., 2004; Pinho et al., 2005; Romero et al., 2005; Burkholder et al., 2019) as their absorption cross sections are similar (Brewer et al., 2019; Burkholder et al., 2019). However, significant uncertainty remains regarding the magnitude of this difference. While acetone photolysis is well-established, MEK quantum yields remain highly uncertain. The IUPAC recommendation for MEK quantum yield at 275–380 nm is 0.34 at 1000 mbar (Raber and Moortgat, 1987), similar to the value of 0.38 used in TUV, yielding photolysis rates approximately 10 times higher than acetone. In contrast, Pinho et al. (2005) derived a value of 0.17 from MEK-NO_x chamber experiments, comparable to the SAPRC-99 value of 0.15 (Carter, 2000). MCM v3.3.1 uses an intermediate value of 0.16.

Considering these studies and the altitude-dependent analysis of Romero et al. (2005), which found MEK photolysis rates approximately 5 times higher than acetone at 0 and 15 km, we increase the MEK photolysis rate by a factor of five in all mechanisms. Photolysis rates for $\geq C_3$ aldehydes in T2 (terpene aldehyde products) are similarly increased by a factor of two, consistent with the treatment of aldehydes in T3.

2.9 Henry's law constants and reactivity factors

Dry and wet deposition processes in CAM-chem require effective Henry's law constants and reactivity factors. The reactivity factor is used for dry deposition with values ranging from 0 to 1, with 1 being as reactive as ozone. For effective Henry's law constants, we prioritize experimental data over theoretical estimates. When available, we use Henry's law constants from JPL Publication 19 (Burkholder et al., 2019), which provides critically evaluated data for key atmospheric species. For species not covered by JPL19, we adopt values from the comprehensive compilation by Sander (2015). When experimental data are unavailable, we estimate Henry's law constants using GROMHE (GROup contribution Method for Henry's law Estimate; Raventos-Duran et al., 2010), a SAR method that predicts solubility based on molecular structure. The temperature dependence of Henry's law constant is characterized by $\Delta H/R$ (enthalpy of dissolution divided by the gas constant). When experimental values of $\Delta H/R$ are unavailable, we assume a value of 6014 K (corresponding to ΔH = 50 kJ mol^{-1}), which is consistent with GECKO-A (Aumont et al., 2005).

Following Schwantes et al. (2020), we assign reactivity factors based on molecular functionality: 1×10^{-36} for non-oxygenated VOCs, 0.1 for species with one oxygenated functional group, and 1.0 for species with two or more oxygenated functional groups. Complete listings of Henry's law constants and reactivity factors for all T3 species are provided in Table S4.

https://doi.org/10.5194/egusphere-2026-1868
Preprint. Discussion started: 29 May 2026

3 Model Configuration and Simulations

3.1 CAM-chem

This study uses the Community Earth System Model (CESM) version 2.2.2 (Danabasoglu et al., 2020), with additional updates applied to its atmospheric component, the Community Atmosphere Model (CAM) version 6.3.133. Among the various configurations available in CESM, we employ CAM-chem, the detailed chemistry configuration of CAM (Emmons et al., 2020).

CESM/CAM-chem supports various horizontal and vertical grid options. We use the spectral element dynamical core (CAM-SE) with a cubed sphere grid at approximately 1-degree resolution globally (ne30pg3), where the grids are created by subdividing each cube face into 30 × 30 elements (Lauritzen et al., 2018), and the elements are divided into 3 × 3 equiangular physics grid cells (Herrington et al., 2019). For vertical levels, we use the 58-layer version, which is expected to be the default number of vertical layers in CESM version 3 (Lauritzen, 2025), instead of the 32 vertical levels used in previous studies (Schwantes et al., 2020; Jo et al., 2023b; Tang et al., 2025).

Horizontal winds (U, V) and temperature (T) are nudged toward the Modern-Era Retrospective analysis for Research and Applications, Version 2 (MERRA-2) reanalysis (Gelaro et al., 2017) with a 3-hour frequency throughout the 2015–2018 period, with the first year results discarded for spin-up.

3.2 Emissions

Biogenic emissions are calculated online in the Community Land Model version 5 (CLM5) using the Model of Emissions of Gases and Aerosols from Nature (MEGAN) v2.1 (Guenther et al., 2012) with satellite-derived plant functional type (PFT) and leaf area index (LAI) from AVHRR and MODIS data (Lawrence and Chase, 2007). We use the extended list of biogenic VOCs implemented in Schwantes et al. (2020) (Table S3 in their paper). For T3, MEGAN emissions are remapped as follows: oxopentanal to C6DIKETONE, pentane to NPENTANE, and all other species previously mapped to BIGALK in T2 are now mapped to C6ALKANES.

For anthropogenic emissions, we use the Community Emissions Data System (CEDS) v2021_04_21 (McDuffie et al., 2020) and the Copernicus Atmosphere Monitoring Service (CAMS-GLOB-ANT) v5.3 (Soulie et al., 2024). While these inventories provide absolute emission amounts for propane, butanes, pentanes, and hexanes and higher alkanes, they do not provide i/n ratios for butanes and pentanes. Therefore, we derive sector-specific i/n ratios from near-source ambient measurements compiled from the literature (Conner et al., 1995; Hwa et al., 2002; Stemmler et al., 2005; Martins et al., 2006; Baker et al., 2008; Lanz et al., 2008; Ho et al., 2009; Gilman et al., 2010, 2013; Simpson et al., 2010, 2014, 2020; Araizaga et al., 2013; Gentner et al., 2013; Swarthout et al., 2013, 2015; Ammoura et al., 2014; Pang et al., 2014; Ait-Helal et al., 2015; Baudic et al., 2016; Dominutti et al., 2016, 2020; Deng et al., 2018; Rossabi and Helmig, 2018; Zhang et al., 2018; Hecobian et al., 2019; Song et al., 2020; Santos and Azevedo, 2021; Wilde et al., 2021), as detailed in Tables S6 and S7. Because transport and energy/industry sectors dominate butane and pentane emissions, we derive separate i/n ratios for these two sectors

https://doi.org/10.5194/egusphere-2026-1868
Preprint. Discussion started: 29 May 2026

along with a general ratio applied to all other sectors. As shown in Table S7, observed i/n ratios vary substantially across studies, but it is apparent that transport sector pentane emissions consistently show much higher i/n ratios than energy/industry emissions. The resulting i/n ratios for butane emissions used in this study are 0.482 (transport), 0.523 (energy/industry), and 0.564 (other sectors). For pentane, the ratios are 2.734 (transport), 1.027 (energy/industry), and 2.037 (other sectors).

Both inventories also report oxygenated VOC (OVOC) emissions by functional groups (e.g., alcohols). CAM-chem applies certain fractions to distribute them to specific species in the model (Emmons et al., 2020). For T3, we derive new speciation fractions for alcohols, aldehydes, and ketones based on measurements made using the NSF NCAR Trace Organic Gas Analyzer (TOGA) (Apel et al., 2015) obtained during various airborne field campaigns (McDuffie et al., 2018; Flocke et al., 2020; Thompson et al., 2022; Pan et al., 2025 ; see Table S8). We also update the fractions used in T1 and T2, as shown in Table S8. The effects of these updated OVOC speciation profiles are discussed in Sect. 4.

For fire emissions, we use the Fire Inventory from NCAR version 2.5 (FINNv2.5) (Wiedinmyer et al., 2023), which provides emissions for MOZART-T1 chemical species. However, it does not provide emissions for newly added T3 species. To generate speciated fire emissions for T3 alkanes, we partition BIGALK emissions using the molar fractions of emission factors for n-butane, i-butane, n-pentane, i-pentane, 2- and 3-methylpentane, n-hexane, and n-heptane reported by Akagi et al. (2011) for each land cover type (Table S9). For land cover types without available data, we use emission factors from the most similar land cover type.

Table 1. Model configurations and chemical mechanism complexity for different MOZART mechanism versions (T1, T2, T3) with two anthropogenic emission inventories (CEDS and CAMS). The number of chemical species, photolysis reactions, and kinetic reactions for each mechanism configuration are shown for each case. Note that the numbers include stratospheric chemistry reactions.

Case name	Mechanism	Anthropogenic Emission	Number of species	Number of photolysis reactions	Number of kinetic reactions
CEDS_T1.2	T1.2	CEDSv2021_04_21	231	123	418
CEDS_T1.3	T1.3	CEDSv2021_04_21	232	124	424
CEDS_T2.3	T2.3	CEDSv2021_04_21	320	168	743
CEDS_T1.3_T3	T3 based on T1.3	CEDSv2021_04_21	278	142	557
CEDS_T2.3_T3	T3 based on T2.3	CEDSv2021_04_21	366	186	876
CAMS_T1.2	T1.2	CAMSv5.3	231	123	418
CAMS_T1.3	T1.3	CAMSv5.3	232	124	424
CAMS_T2.3	T2.3	CAMSv5.3	320	168	743
CAMS_T1.3_T3	T3 based on T1.3	CAMSv5.3	278	142	557
CAMS_T2.3_T3	T3 based on T2.3	CAMSv5.3	366	186	876

https://doi.org/10.5194/egusphere-2026-1868
Preprint. Discussion started: 29 May 2026

3.3 Simulation Cases

In this study, while we focus on changes in global VOCs and OVOCs due to chemical mechanism updates, we also examine the impacts of anthropogenic emission inventory selection to compare the effects of chemical mechanism uncertainty against emission inventory uncertainty. Five simulation cases are set up with different chemical mechanism configurations, and two different emission inventories are used for each case, resulting in 10 simulations total, as shown in Table 1.

Table 2. Global annual anthropogenic emissions (Tg yr^{-1}) by species for CEDS v2021_04_21 and CAMS v5.3 inventories used in model simulations, averaged over 2016–2018. Only VOC species relevant to this study are listed; other NMVOCs such as aromatics and alkenes are excluded. NMVOC represents the total non-methane volatile organic compound emissions from each inventory, including all speciated and unspeciated VOCs. BC and OC refer to black carbon and organic carbon aerosols, respectively. NO_x emissions are calculated assuming a molecular weight of NO.

Species	CEDS	CAMS
Ethane	5.2	4.7
Propane	4.8	6.2
Butanes	12.6	9.5
Pentanes	15.4	5.0
Hexanes	26.0	21.3
Alcohols	6.1	15.5
Aldehydes	1.8	9.3
Ketones	3.8	7.9
Formaldehyde	2.0	4.4
NMVOC	148.4	144.8
BC	5.9	4.7
OC	13.8	11.7
SO_2	85.7	95.6
CO	540.1	567.2
NO_x	77.7	77.5

https://doi.org/10.5194/egusphere-2026-1868
Preprint. Discussion started: 29 May 2026

4 Global Budget and Distribution

This section examines how more comprehensive alkane chemistry in T3 affects global budgets and distributions of VOCs and OVOCs. We compare T1, T2, and T3 mechanisms by analyzing monthly time series, vertical profiles, and spatial distributions. To separate chemistry-driven changes from emission-driven variability, we also evaluate differences between CEDS and CAMS anthropogenic emission inventories. The analysis covers primary alkanes (C3H8 and BIGALK) and their oxidation products (ketones, aldehydes, and organic nitrates), assessing whether mechanism choice or emission inventory selection has a greater influence on the budget variations for each species group.

4.1 Propane

Although the total reaction rate of C3H8 with OH is consistent across all mechanisms, T3 introduces explicit treatment of propyl peroxy radical isomers and their distinct oxidation products (propanal, propanol, and PPN). The global burden of propane shows minimal sensitivity to mechanism choice (<5% variation between cases), while emission inventory selection drives much larger differences (~20% variation: 231–241 Gg for CEDS vs. 285–297 Gg for CAMS) (Table 2). However, the key advantage of T3 lies in its ability to explicitly track hydrogen abstraction sites on the propane molecule. This explicit tracking enables improved evaluation of altitude-dependent formation of acetone and related OVOCs, which cannot be assessed in lumped mechanisms. Global simulations quantify the branching ratios at 75% for secondary carbon and 25% for primary carbon hydrogen abstraction. Additionally, T3 demonstrates that the fraction of secondary carbon hydrogen abstraction increases with altitude (Fig. S1), indicating relatively enhanced acetone formation at higher altitudes.

4.2 BIGALK (NBUTANE, ISOBUTANE, NPENTANE, IPENTANE, C6ALKANES)

Figure 3 shows the global burden time series of BIGALK across T1, T2, and T3, along with the relative contributions of individual species. Although BIGALK is divided into five distinct alkane species with different OH reaction rates in T3, the total $\geq C_4$ alkane global budgets remain remarkably consistent across mechanisms (Fig. 3b), indicating that the average reaction rate constant for BIGALK assumed in T1 and T2 performs well globally. Similar to propane, emission inventory selection drives larger variations in BIGALK burden than mechanism choice (Fig. 3a). T3 resolves the contributions of individual alkanes to OH reactivity (Fig. 3c), while maintaining total reactivity consistent with T1 and T2. T3 produces higher BIGALK mixing ratios over remote regions (Fig. 3f) and in the free troposphere (Fig. 3i), indicating that explicitly resolving individual alkane species results in longer lifetimes for less reactive species (C_4) despite enhanced removal of more reactive species (C_6). Vertical profiles of individual alkanes (Fig. S2) confirm this behavior, showing that C_6 alkanes dominate in the boundary layer while lighter alkanes (C_4–C_5) become relatively more important at higher altitudes due to their longer lifetimes. Note that T2 also shows differences in BIGALK concentrations near biogenic source regions (Fig. 3e, h) because T2 includes updated isoprene and terpene chemistry which affects OH concentrations in these regions. In summary, T3 maintains global budget consistency with T1 and T2 while capturing more detailed spatial and vertical distributions of individual alkane species.

https://doi.org/10.5194/egusphere-2026-1868
Preprint. Discussion started: 29 May 2026

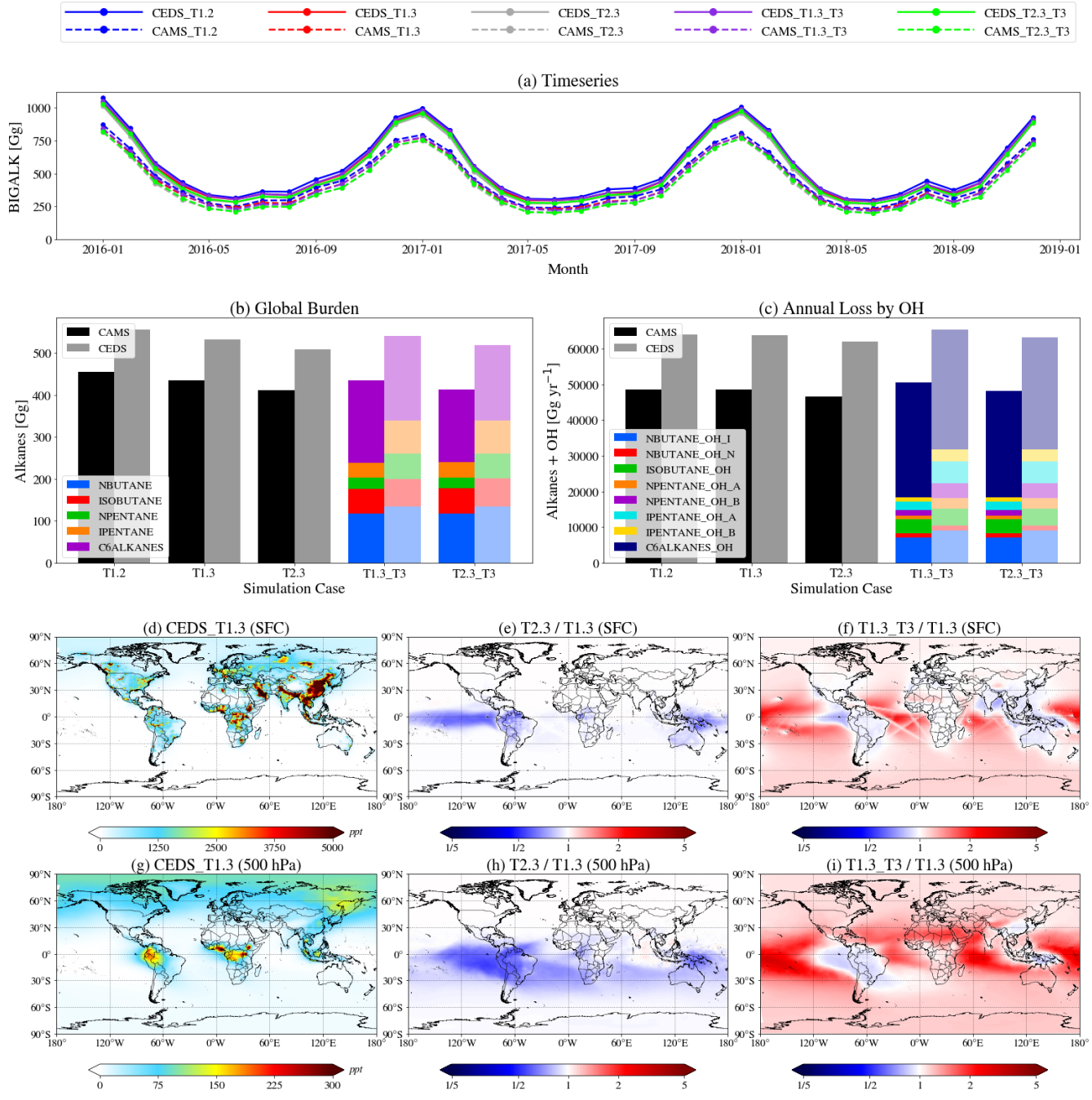

355 **Figure 3.** (a) Monthly time series of global BIGALK burden. (b) Annual mean global BIGALK burden with speciated contributions in T3. (c) Annual total BIGALK+OH reaction rates with speciated contributions in T3. Annual mean BIGALK mixing ratios at (d) the surface and (g) 500 hPa. Ratio of BIGALK between CEDS_T2.3 and CEDS_T1.3 at (e) the surface and (h) 500 hPa. Ratio of BIGALK between CEDS_T1.3_T3 and CEDS_T1.3 at (f) the surface and (i) 500 hPa.

https://doi.org/10.5194/egusphere-2026-1868
Preprint. Discussion started: 29 May 2026

4.3 Ketones (CH3COCH3, MEK, PENTANONE2, PENTANONE3, NELSON, HYDROXYKETONE, C6KETOOH, C6DIKETONE)

Figure 4 shows the global burden of ketones across different mechanisms and emission inventories. While T1 and T2 simulate acetone (CH3COCH3) and MEK as the primary ketone species, T3 introduces six additional C_5–C_6 ketones (PENTANONE2, PENTANONE3, NELSON, HYDROXYKETONE, C6KETOOH, and C6DIKETONE; see Table S3 for chemical formulas). Unlike C3H8 and BIGALK, ketone budgets are more sensitive to chemical mechanism choice than emission inventory selection. As shown in Table S10, global acetone burden decreases by ~23% in T2 compared to T1 due to updated terpene chemistry (Schwantes et al., 2020), which reduces acetone chemical production. Although T3 increases acetone chemical production slightly (0.41–3.06 Tg yr^{-1}) through multiple acetone production channels from anthropogenic species, the T2 terpene updates dominate the overall acetone budget changes.

MEK burden is dramatically reduced in T1.3 and further decreased in T1.3_T3 compared to T1.2. Three major factors contribute to this reduction (Table S10). The most important is that T3 explicitly represents MEK formation from n-butane oxidation rather than using the lumped BIGALK approach, leading to a factor of 4–5 decrease in MEK chemical production (Table S10). In T1 and T2, MEK forms from the BIGALK alkoxy radical pathway (via HO_2 generation channel) with a fixed yield of 0.8. However, this yield overestimates MEK production because n-butane (the primary MEK precursor) contributes far less than 80% to total BIGALK mass (Sect. 4.2). The second most important factor is increased MEK photolysis rates, which decrease its atmospheric lifetime by ~30%. Finally, VOC emission speciation ratios are adjusted based on TOGA measurements over source regions, reducing MEK emissions. The latter two changes are incorporated into T1.3 and T2.3. Since chemical production dominates over anthropogenic emissions, adjusting ketone speciation emission ratios has minimal impact on the global MEK budget.

T3 introduces six additional C_5–C_6 ketone species that were not explicitly represented in previous MOZART mechanisms. PENTANONE2 and PENTANONE3 are formed through n-pentane oxidation pathways with different hydrogen abstraction positions. NELSON (methyl isopropyl ketone) forms from i-pentane oxidation. HYDROXYKETONE represents hydroxy-substituted ketones formed during $\geq C_6$ alkane oxidation via hydrogen-shift reactions. C6KETOOH, formed through hydrogen shifts from peroxy radicals followed by O_2 addition, represents a hydroperoxy ketone species. C6DIKETONE is primarily formed through oxidation of C6KETOOH and HYDROXYKETONE, with minor contributions from biogenic sources. These six C_5–C_6 ketones contribute ~40% to global total ketone sources in T3 but only ~2% to the total ketone burden due to their short atmospheric lifetimes (Fig. 4a, Table S10).

Comparing total chemical production and burden across mechanisms reveals two major factors driving the ketone budget differences. First, acetone chemical production and burden decrease significantly in T2 (~25%), representing the dominant change in total ketone budgets. This decrease is primarily driven by differences in monoterpene oxidation pathways between T1 and T2, where T2 reduces CH3COCH3 yields from both ozonolysis and OH-initiated oxidation of monoterpenes (see Table S6 in Schwantes et al., 2020 and Table S2 in Emmons et al., 2020 for more details). Second, while adding C_5–C_6 ketones increases global ketone chemical production by ~30% in T3, the total burden decreases slightly because these higher-

https://doi.org/10.5194/egusphere-2026-1868
Preprint. Discussion started: 29 May 2026

carbon ketones have shorter atmospheric lifetimes, reducing the average ketone lifetime. Overall, mechanism choice has a larger impact on ketone budgets than emission inventory selection, contrasting with the simulated behavior of alkanes (C3H8 and BIGALK).

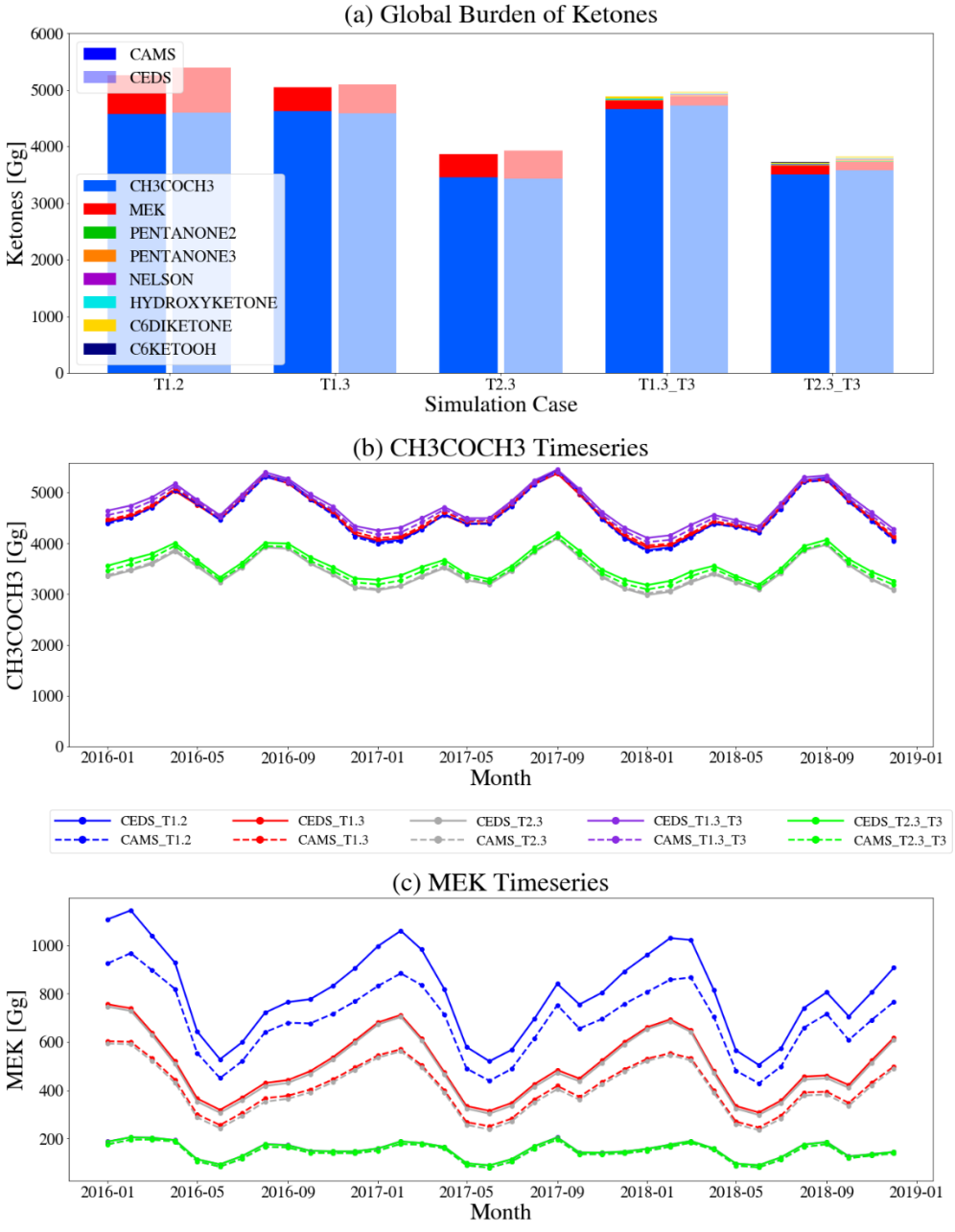

Figure 4. (a) Annual mean global burden of ketones showing individual C_3–C_6 ketone species contributions. (b-c) Monthly time series of global (b) CH3COCH3 and (c) MEK burdens across different mechanisms and emission inventories. In (c), the CEDS/CAMS_T1.3_T3 lines (purple) closely overlap with the CEDS/CAMS_T2.3_T3 lines (green).

https://doi.org/10.5194/egusphere-2026-1868
Preprint. Discussion started: 29 May 2026

4.4 Aldehydes (CH3CHO, PROPANAL, BUTANAL)

While T1 and T2 use acetaldehyde (CH3CHO) as a lumped surrogate for aldehydes derived from $\geq C_2$ alkane oxidation, T3 explicitly represents propanal and butanal from propane and butane oxidation, respectively. Compared to acetaldehyde, propanal and butanal have much smaller atmospheric burdens (Table S11), justifying the computational efficiency of the lumped approach in T1 and T2. However, T3 chemistry modifies acetaldehyde concentrations by changing its production pathways from $\geq C_4$ alkanes. The chemical production of acetaldehyde varies by up to ~16% across mechanisms (T1.2 vs. T2.3_T3), exceeding the <5% variation from emission inventory selection. T3 decreases acetaldehyde concentrations because the effective yield is lower than the fixed yield assumed in T1 and T2. In T1 and T2, acetaldehyde forms from BIGALK alkoxy radicals (via RO2+NO reactions or hydroperoxide photolysis) with a fixed yield of 0.4. In contrast, T3 applies compound-specific yields, and some alkanes such as i-butane produce no acetaldehyde. Consequently, the global acetaldehyde burden decreases by 8–14% in T3 compared to T1 and T2 (Table S11).

Propanal, explicitly represented only in T3 through propane oxidation, exhibits distinct characteristics compared to acetaldehyde. While acetaldehyde shows relatively weak seasonal variation (Fig. 5a) due to its multiple sources including biomass burning and biogenic sources, propanal displays pronounced seasonality with higher burdens during Northern Hemisphere winter and lower burdens in summer (Fig. 5b), reflecting the seasonal cycle of propane. Butanal, derived only from n-butane oxidation, shows similar patterns to propanal (not shown) but with even smaller atmospheric burdens due to its shorter lifetime (Table S11). These characteristics are also reflected in their spatial distributions (Fig. 5c-d), where propanal shows stronger anthropogenic patterns while acetaldehyde reflects contributions from multiple sources.

https://doi.org/10.5194/egusphere-2026-1868
Preprint. Discussion started: 29 May 2026

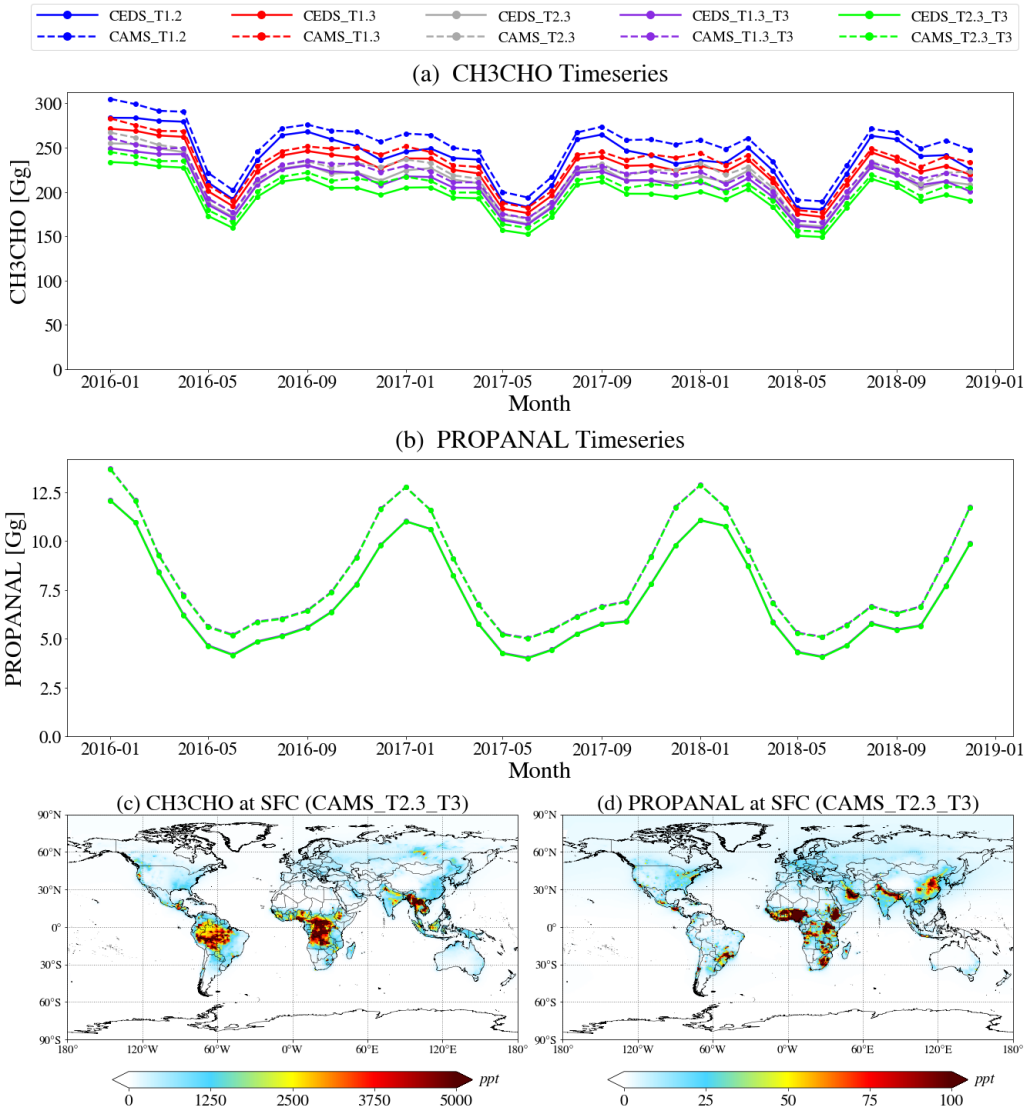

Figure 5. Monthly time series of global burden for (a) CH3CHO and (b) PROPANAL. Annual mean surface mixing ratios of (c) CH3CHO and (d) PROPANAL from the CAMS_T2.3_T3 simulation. Note that PROPANAL is only explicitly represented in T3 mechanism. In (b), the CEDS/CAMS_T1.3_T3 lines (purple) closely overlap with the CEDS/CAMS_T2.3_T3 lines (green).

4.5 Organic Nitrates (PAN, PPN, and ALKNIT)

Similar to acetaldehyde, PAN burden decreases in T3 compared to T1 and T2 (Fig. 6a), as acetaldehyde is one of PAN's key precursors. However, the magnitude of PAN burden reduction in T3 relative to T1 and T2 is smaller than that of acetaldehyde (7–9% for PAN vs. 8–14% for acetaldehyde). This difference occurs because the peroxyacetyl radical (CH_3CO_3), which reacts with NO_2 to form PAN, is generated not only from acetaldehyde oxidation but also from other pathways such as biogenic VOC oxidation and photolysis of ketones.

https://doi.org/10.5194/egusphere-2026-1868
Preprint. Discussion started: 29 May 2026

PPN, explicitly simulated only in T3 as a product of propanal oxidation, represents a small contribution to the total organic nitrate budget. With a global burden of 40–50 Gg, PPN represents only ~2% of PAN burden (2000–2300 Gg, Table S11), justifying its omission in computationally efficient mechanisms like T1. However, explicit representation of PPN in the MOZART-T3 mechanism enables more comprehensive model evaluation against observational datasets as discussed in Sect. 5.

T3 more comprehensively represents alkyl nitrates from individual alkane oxidation pathways. While T1 and T2 simulate ALKNIT as a lumped species from BIGALK oxidation, T3 produces compound-specific alkyl nitrates from C_2–C_6 alkanes. Despite this increased chemical detail, total ALKNIT burden shows small variation across mechanisms, with up to 20–24% difference between T1.2 and T1.3_T3, and only 7–10% between T1.3 and T1.3_T3 (Table S10). Among the C_2–C_6 species, C_6 compounds (C6ALKO2 and C6ALKOHO2) dominate ALKNIT chemical production (Fig. S3), contributing more than half (54% in CEDS and 60% in CAMS), consistent with the general increase in alkyl nitrate yields with carbon number as discussed in Sect. 2.3 (Arey et al., 2001; Jenkin et al., 2019). Despite the very low alkyl nitrate branching ratio from ethyl peroxy radical (Fig. S4), ethyl peroxy radicals produced from decomposition of higher carbon number alkoxy and peroxy radicals (e.g., from isopentane oxidation), as well as from ethane oxidation, collectively contribute 9–10% to total ALKNIT chemical production.

T3's explicit representation fundamentally alters the spatiotemporal patterns of ALKNIT. Rather than uniformly scaling concentrations, T3 produces stronger seasonal variations with pronounced NH winter maxima and NH summer minima (Fig. 6c). The vertical distribution also shifts dramatically: T3 simulates higher ALKNIT at the surface but lower ALKNIT at 200 hPa compared to T1 (Fig. S5). These contrasting patterns arise from fundamentally different chemistry in the two mechanisms. T1 relies on a single BIGALK pathway to produce ALKNIT (Fig. S3), whereas T3 employs 13 distinct pathways, each with unique precursor lifetimes and nitrate yields. This mechanistic complexity is evident in the altitude dependence of alkyl nitrate formation. In T1, only temperature affects ALKNIT production rates (Emmons et al., 2020), causing branching ratios to increase monotonically with altitude as temperature decreases (Fig. S4). In contrast, T3 incorporates both temperature and pressure dependencies following Jenkin et al. (2019), where decreasing air density at higher altitudes partially offsets the temperature effect, suppressing nitrate yields in the upper troposphere. Additionally, as discussed in Sect. 4.2 (Fig. S2), higher carbon alkanes have shorter lifetimes and thus lower concentrations in the upper troposphere. Consequently, T3 redistributes ALKNIT toward lower altitudes compared to T1, which may influence NO_x partitioning and transport. The ALKNIT distribution shift in T3 thus reflects the complex interplay of VOC speciation from emission inventories, precursor lifetimes, and temperature- and pressure-dependent branching ratios—factors that cannot be captured by a single lumped species.

https://doi.org/10.5194/egusphere-2026-1868
Preprint. Discussion started: 29 May 2026

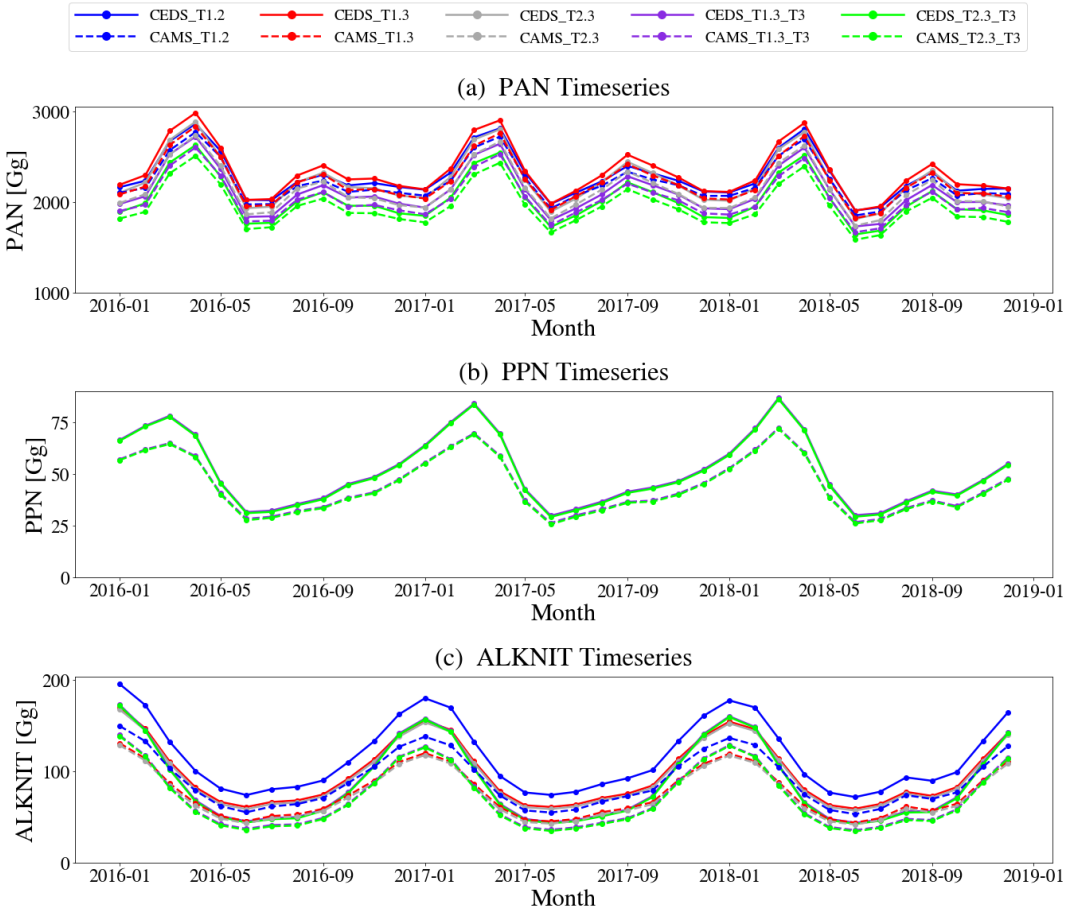

Figure 6. Monthly time series of global burden for (a) PAN, (b) PPN, and (c) ALKNIT across different mechanisms and emission inventories.

https://doi.org/10.5194/egusphere-2026-1868
Preprint. Discussion started: 29 May 2026

5 Comparison with ATom observations

To illustrate the value of representing butanes and pentanes and their oxidation products, we evaluate the model simulations against global observations to assess the performance of different mechanisms in CAM-chem. While much of the new chemistry of T3 occurs near source regions, it also improves the representation of long-lived oxidation products (e.g., MEK) in the remote atmosphere. We focus on VOCs and OVOCs whose production and loss processes are added or modified in the T3 mechanism, as well as major air pollutants such as ozone, NO_x, HO_x, and formaldehyde.

The ATom mission conducted airborne measurements over the Pacific and Atlantic Ocean basins during four deployments spanning different seasons from 2016 to 2018 (Thompson et al., 2022). ATom specifically targeted the remote atmosphere, which is distant from, but still influenced by, anthropogenic pollution sources. This makes ATom observations particularly suitable for evaluating global chemical mechanisms, as the remote atmosphere allows us to assess the long-range transport and chemical evolution of pollutants without the complexity of local influences. The campaign measured a comprehensive suite of VOCs and OVOCs relevant to this study, including alkanes, aldehydes, ketones, and organic nitrates, along with major air pollutants. With measurements spanning from the surface to the upper troposphere (~12 km) across four seasons and two ocean basins, ATom provides systematic global coverage for evaluating both spatial distributions and seasonal variations simulated by global atmospheric chemistry models such as CAM-chem. For species with measurements below their detection limits, we assign a value of zero rather than excluding those data points, to avoid sampling biases toward higher concentrations.

We first evaluate general model performance for major air pollutants and oxidants including ozone, NO, NO_2, CO, OH, HO_2, formaldehyde, and acetaldehyde (Fig. S6). Overall, the model captures the observed vertical distributions reasonably well across different altitude bins, indicating that CAM-chem successfully reproduces the average oxidation conditions and meteorological fields of the global atmosphere during ATom. CO is underestimated, especially in the lower troposphere, consistent with pervasive negative biases of CO reported in previous global chemistry model studies (Stein et al., 2014; Huang et al., 2016; Emmons et al., 2020; Gaubert et al., 2020). OH and HO_2 are generally well captured within the observed variability, showing good agreement across most altitude bins. Acetaldehyde is significantly underestimated across all model cases, consistent with a known missing source in the remote troposphere. Wang et al. (2019) showed that oceanic emissions primarily affect the marine boundary layer, while organic aerosol photolysis can only partially explain the gap in the free troposphere, suggesting the existence of additional unidentified gas-phase precursors.

Importantly, all model cases show similar performance for these major pollutants and oxidants, with differences between emission inventories generally larger than those between chemical mechanisms. This suggests that additional speciated alkane chemistry does not significantly affect major air pollutant simulations at the global scale, confirming that the T1 mechanism adequately captures atmospheric chemistry without detailed alkane speciation, at least in terms of global averages. While the impacts of detailed alkane chemistry in polluted urban areas will be evaluated using higher horizontal resolution (~7 km) simulations such as Multi-Scale Infrastructure for Chemistry and Aerosols (MUSICA, Pfister et al., 2020;

https://doi.org/10.5194/egusphere-2026-1868
Preprint. Discussion started: 29 May 2026

Jo et al., 2023b), this result suggests that studies primarily interested in global-scale major pollutant concentrations can use the T1 mechanism without requiring detailed alkane speciation.

In contrast to major air pollutants, alkanes and their OVOC products show more distinct differences among model cases (Fig. 7). Propane and $\geq C_4$ alkanes show underestimations with normalized mean biases (NMBs) of -65 to -73% for propane and -32 to -53% for $\geq C_4$ alkanes. Note that applying exact detection limit values instead of zero for below-detection-limit measurements changes these NMBs by only ~1% for propane and ~7% for $\geq C_4$ alkanes, indicating that this choice does not significantly affect the results. The differences among chemical mechanisms (T1, T2, T3) are minimal for propane, as expected since only the oxidation pathways differ among mechanisms while the reaction rate of propane with OH remains unchanged. This is also the case for $\geq C_4$ alkanes, as OH levels are similar and the reaction rate for BIGALK in T1 is comparable to the average reaction rate of $\geq C_4$ alkanes in T3. Nevertheless, T3 slightly improves the $\geq C_4$ alkane bias by ~5%. In contrast, $\geq C_6$ alkanes (available only in T3) show overestimation with NMBs of 132 to 170%. However, these NMBs are greatly reduced to 22 to 41% when below-detection-limit measurements are set to their detection limit values instead of zero, as a large fraction of $\geq C_6$ alkane measurements fall below the detection limit. Given that TOGA does not report all C_6 alkane species (TOGA measured five $\geq C_6$ alkanes during ATom: 2-methylpentane, 3-methylpentane, n-hexane, n-heptane, and 2,2,4-trimethylpentane) and that $\geq C_6$ alkanes concentrations are lower than propane and $\geq C_4$ alkanes by a factor of ~10 (Fig. 7), the apparent overestimation likely reflects uncertainties in both the observations and the VOC speciation in emission inventories.

When examining individual C_4–C_5 alkane species (Fig. S7), all species (n-butane, i-butane, n-pentane, and i-pentane) show similar underestimation patterns (NMBs of -14% to -67%). However, the ratios of branched to total alkanes (i-butane/butanes and i-pentane/pentanes) are well captured by the model, with mean ratio differences of less than 0.04 (~10%) for both butanes and pentanes. This agreement validates the i/n emission ratios presented in Tables S6 and S7 and the reaction rates with OH, suggesting that while absolute emission magnitudes may be underestimated, the relative composition of alkane isomers is reasonably represented in the model.

PAN concentrations are relatively well captured across all model cases and altitude bins, with model results following the observed vertical distributions. However, all model cases tend to overestimate upper troposphere values. The degree of overestimation decreases with increasing chemical complexity: NMBs are 68–80% for T1.2 and T1.3 cases, 61–72% for T2.3 cases, 54–61% for T1.3_T3 cases, and 47–54% for T2.3_T3 cases.

Unlike PAN, PPN concentrations are substantially underestimated with NMBs of -66 to -72%. This underestimation may be due to underestimated propanal levels, a precursor of PPN, with models showing an NMB of -75% for propanal. In contrast, acetone shows good agreement with observations, especially when using T2.3_T3 chemistry (NMB of -1% to 1%). Because the lifetime of propanal (less than a day) is much shorter than that of acetone (~12 days), propanal concentrations can be more strongly affected by available propane. The ratios between OVOCs (acetone, PPN, and propanal) and their parent

https://doi.org/10.5194/egusphere-2026-1868
Preprint. Discussion started: 29 May 2026

hydrocarbon (propane) show different patterns (Fig. S7): overestimation of the acetone-to-propane ratio and underestimation of the propanal-to-propane and PPN-to-propane ratios.

Among the OVOCs, MEK shows the most pronounced differences between mechanisms, as discussed in Sect. 4.3. The model results fall into three distinct groups: the base mechanism (T1.2), T1.3 and T2.3 with updates from this study (Sect. 2.8 – updates to photolysis rates and OVOC emission ratios), and T3 cases (T1.3_T3 and T2.3_T3). The base mechanism (T1.2) significantly overestimates MEK concentrations throughout the vertical profile, while T1.3 and T2.3 show much better agreement with observations. However, these cases still overestimate MEK above 3 km altitude, and these overestimations shift to underestimations when the new chemistry in T3 is added. The NMBs are 302–374% for T1.2, 117–173% for T1.3 and T2.3, and -29 to -33% for all T3 cases.

While these updates bring MEK into reasonable agreement with observations in terms of NMB, detailed evaluation reveals a more complex situation (Fig. S8). The evaluation results differ by individual ATom campaign and by region. For example, T3 cases show good agreement with observations for ATom-2, but T1 and T2 with photolysis rate updates show better agreement for ATom-4. Regional evaluation also shows varying performance. One consistent finding is that the base configuration (T1.2) without any updates always shows substantial overestimation for each campaign and region, regardless of the emission inventory used. Comparison over the North America domain shows better agreement for T3 cases, and given that n-butane (a MEK precursor) is also underestimated during ATom, this may indicate that the T3 chemical mechanism is accurate in terms of MEK.

Finally, we evaluate alkyl nitrates from alkane oxidation (ALKNIT). The model ALKNIT represents the sum of all alkyl nitrates produced from alkane oxidation pathways. ATom measurements of isopropyl nitrate, a single alkyl nitrate species from propane oxidation, show mixing ratios comparable to or even higher than the total model ALKNIT, indicating substantial underestimation of total alkyl nitrates in the model. In contrast, the model simulates approximately three times higher ALKNIT values below 3 km over North America (not shown), suggesting that photolysis rates or OH reaction rates of alkyl nitrates may need to be revisited in future studies. However, given that precursor alkanes (propane and $\geq C_4$ alkanes) are also underestimated, it is difficult to attribute the ALKNIT underestimation solely to chemistry, as emission uncertainties may also contribute.

https://doi.org/10.5194/egusphere-2026-1868
Preprint. Discussion started: 29 May 2026

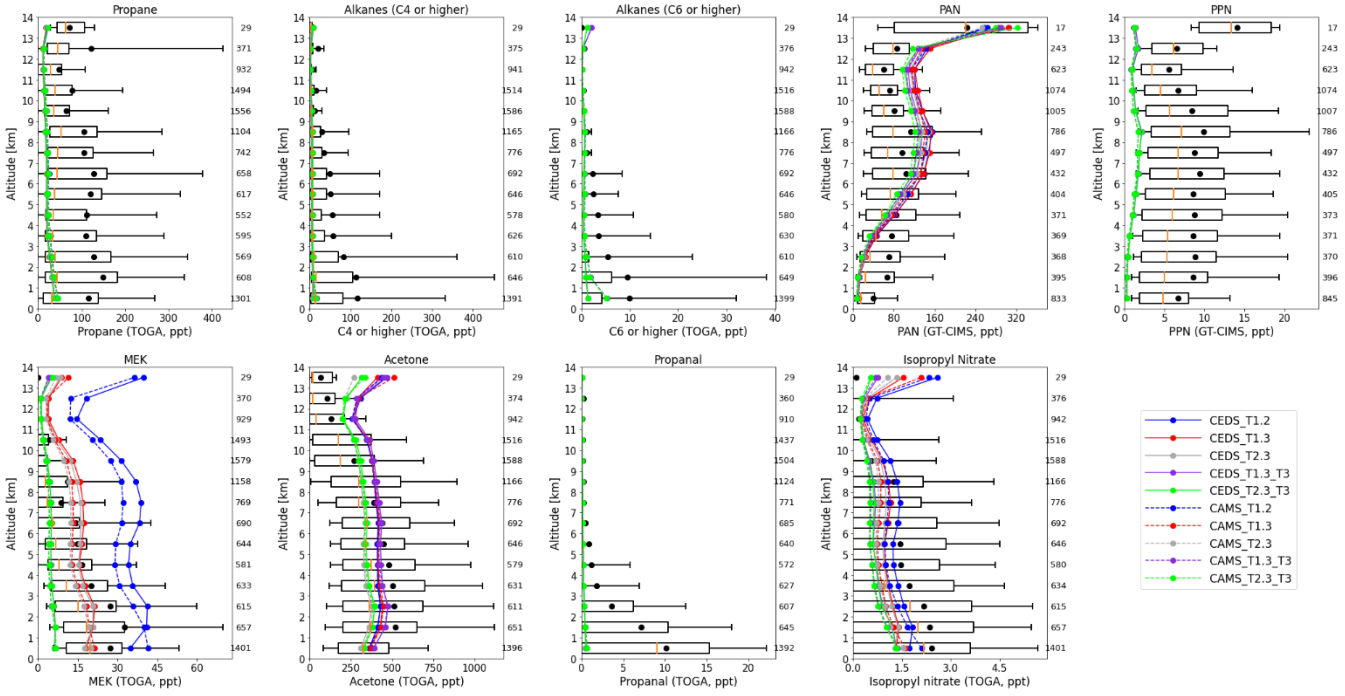

Figure 7. Vertical profiles of alkanes (propane, C_4 or higher, C_6 or higher), PANs (PAN, PPN), and OVOCs (MEK, acetone, propanal, isopropyl nitrate) compared with ATom observations. Box-and-whisker plots show the distribution of ATom measurements at each altitude bin, with the box representing the interquartile range, the orange line indicating the median, and whiskers extending to the 10th and 90th percentiles. Black dots represent the mean of observations. Model median values from different mechanism and emission inventory combinations are shown as colored lines and symbols. Numbers on the right *y*-axis indicate the number of observations in each altitude bin. Note that PPN and propanal are represented only in T3 mechanism, and the model results for isopropyl nitrate represent total lumped alkyl nitrates (ALKNIT) for approximate comparison with observations.

6 Conclusions

This study presents MOZART-T3, an atmospheric chemistry mechanism that replaces the lumped alkane compound (BIGALK) representation in MOZART-T1 and T2 with more comprehensive treatment of individual C_4–C_6 alkane species. T3 also implements more detailed propane chemistry by resolving propyl peroxy radical isomers. This more comprehensive representation fundamentally alters how alkane oxidation and alkane-derived OVOCs are simulated in CAM-chem, enabling more mechanistically consistent evaluation of these species.

Global budget analyses show that T3 maintains consistency with T1 and T2 for total alkane burdens while providing mechanistic detail that enables more comprehensive model evaluation. For propane, T3 quantifies hydrogen abstraction branching ratios at 75% for secondary carbon and 25% for primary carbon, with the secondary fraction increasing with altitude. For ≥C_4 alkanes, T3 demonstrates that the lumped BIGALK approach in T1 and T2 adequately captures average global reactivity, but the more comprehensive representation can simulate altitude-dependent distributions driven by species-specific lifetimes.

https://doi.org/10.5194/egusphere-2026-1868
Preprint. Discussion started: 29 May 2026

The oxidation products of alkanes show greater sensitivity to mechanism choice than the parent alkanes. In particular, MEK shows the most pronounced mechanism differences, with T3 reducing MEK burden substantially compared to T1 through three factors: adjusted emission speciation ratios, increased photolysis rates, and explicit representation of n-butane oxidation. T3 introduces six additional C_5–C_6 ketone species that contribute approximately 40% to global ketone sources but only 2% to total ketone burden due to their short atmospheric lifetimes. For aldehydes, T3 decreases acetaldehyde burden by 8–14% through compound-specific yields that replace the fixed 0.4 yield in T1 and T2, while explicitly representing propanal and butanal.

Evaluation against ATom observations demonstrates that all mechanisms adequately capture major air pollutants and oxidants (e.g., O_3, NO_x, and HO_x) at the global scale, with emission inventory differences generally exceeding mechanism differences. However, T3 enables evaluation of species not previously represented, including individual C_4–C_6 alkanes, propanal, and PPN. The model captures observed i/n ratios for butanes and pentanes well, validating the emission ratios and OH reaction rates, though absolute alkane concentrations are underestimated. MEK evaluation reveals complex spatial and temporal variability, with T3 showing improved performance but results vary by region and season.

The development of T3 represents a balance between chemical complexity and computational efficiency. While T3 adds detail for alkane oxidation, it demonstrates that lumped approaches in T1 and T2 adequately represent global-scale major pollutant concentrations. However, the explicit treatment in T3 enables more comprehensive evaluation against observations, particularly for OVOCs that are increasingly measured in field campaigns.

This study focuses on global-scale evaluation of the T3 mechanism as a necessary first step in mechanism development. However, the impact of detailed alkane chemistry is expected to be more pronounced in polluted urban environments or biomass burning hot spots, where VOC concentrations and photochemical activity are substantially higher. Future work should prioritize evaluating T3 performance in urban areas using higher-resolution regional simulations such as MUSICA, where the explicit representation of individual alkane species and their oxidation products may more significantly affect ozone and secondary pollutant formation. Such high-resolution urban simulations will provide critical insights into whether the added chemical complexity in T3 translates to improved air quality predictions in populated regions. Additionally, this study reveals substantial underestimation of alkane concentrations in both CEDS and CAMS emission inventories, suggesting that alkane emissions need to be revisited. The explicit representation of individual alkane species and their isomer ratios in T3 provides a valuable tool for diagnosing missing emission sources, as isomer ratios can help distinguish between different source types. Improving emission inventories in conjunction with more detailed chemical mechanisms such as T3 will be essential for accurately simulating alkane chemistry and its impacts on ozone and secondary pollutant formation across different environments.

https://doi.org/10.5194/egusphere-2026-1868
Preprint. Discussion started: 29 May 2026

Code and Data Availability. Community Earth System Model is an open-source community model and is publicly available at https://github.com/ESCOMP/CESM. The chemical mechanism files used in this study are available on the Zenodo repository (https://doi.org/..... to be assigned upon publication). Global simulation output used in this study has been archived and is available from the corresponding author upon request. ATom measurements are publicly available at NASA Earthdata: https://www.earthdata.nasa.gov/data/projects/atom.

Author Contributions. DSJ, JJO, RHS, and LKE designed the research and developed the T3 mechanism. JJO calculated the fraction of hydrogen shift reactions for ≥C_6 alkanes. RSH and ECA derived new OVOC speciation ratios for anthropogenic emissions. DSJ and RSH derived i/n ratios of butanes and pentanes for anthropogenic emissions, and RHS derived those for biomass burning emissions. DSJ, ECA, and KU derived new photolysis rates for higher carbon aldehydes and ketones. RSH, ECA, AJH, LGH, CRT, and JP provided ATom measurements used in this study. CG provided the CAMS anthropogenic emission inventory. DSJ, RHS, and LKE conducted global simulations using CAM-chem. DSJ wrote the manuscript with contributions from all coauthors.

Acknowledgments. This work was supported by the National Research Foundation of Korea (NRF) grant funded by the Korea government (MSIT) (RS-2025-00513391). This work was also supported by the NSF National Center for Atmospheric Research, which is a major facility sponsored by the U.S. National Science Foundation under Cooperative Agreement No. 1852977, and NASA Awards 80NSSC18K0681, 80NSSC21K1439, and NNX15AG70A. This work was also supported in part by NOAA cooperative agreement NA22OAR4320151. We would like to acknowledge high-performance computing support from the Derecho system (doi:10.5065/qx9a-pg09) provided by the NSF National Center for Atmospheric Research, sponsored by the U.S. National Science Foundation. We would like to thank William H. Brune, Kathryn McKain, Colm Sweeney, and Thomas B. Ryerson for providing OH and HO_2 (Brune et al., 2021), CO (McKain and Sweeney, 2021), NO, NO_2, and O_3 (Ryerson et al., 2019) measurements during the ATom campaign. We also thank Samuel R. Hall for helpful discussions on photolysis rates.

Competing Interests. The authors declare that they have no competing interests.

https://doi.org/10.5194/egusphere-2026-1868
Preprint. Discussion started: 29 May 2026

References

Ait-Helal, W., Beeldens, A., Boonen, E., Borbon, A., Boréave, A., Cazaunau, M., Chen, H., Daële, V., Dupart, Y., Gaimoz, C., Gallus, M., George, C., Grand, N., Grosselin, B., Herrmann, H., Ifang, S., Kurtenbach, R., Maille, M., Marjanovic, I., Mellouki, A., Miet, K., Mothes, F., Poulain, L., Rabe, R., Zapf, P., Kleffmann, J. and Doussin, J.-F.: On-road measurements of NMVOCs and NOx: Determination of light-duty vehicles emission factors from tunnel studies in Brussels city center, Atmos. Environ., 122, 799–807, doi:10.1016/j.atmosenv.2015.09.066, 2015.

Akagi, S. K., Yokelson, R. J., Wiedinmyer, C., Alvarado, M. J., Reid, J. S., Karl, T., Crounse, J. D. and Wennberg, P. O.: Emission factors for open and domestic biomass burning for use in atmospheric models, Atmos. Chem. Phys., 11(9), 4039–4072, doi:10.5194/acp-11-4039-2011, 2011.

Ammoura, L., Xueref-Remy, I., Gros, V., Baudic, A., Bonsang, B., Petit, J.-E., Perrussel, O., Bonnaire, N., Sciare, J. and Chevallier, F.: Atmospheric measurements of ratios between CO_2 and co-emitted species from traffic: a tunnel study in the Paris megacity, Atmos. Chem. Phys., 14(23), 12871–12882, doi:10.5194/acp-14-12871-2014, 2014.

Apel, E. C., Emmons, L. K., Karl, T., Flocke, F., Hills, A. J., Madronich, S., Lee-Taylor, J., Fried, A., Weibring, P., Walega, J., Richter, D., Tie, X., Mauldin, L., Campos, T., Weinheimer, A., Knapp, D., Sive, B., Kleinman, L., Springston, S., Zaveri, R., Ortega, J., Voss, P., Blake, D., Baker, A., Warneke, C., Welsh-Bon, D., de Gouw, J., Zheng, J., Zhang, R., Rudolph, J., Junkermann, W. and Riemer, D. D.: Chemical evolution of volatile organic compounds in the outflow of the Mexico City Metropolitan area, Atmos. Chem. Phys., 10(5), 2353–2375, doi:10.5194/acp-10-2353-2010, 2010.

Apel, E. C., Hornbrook, R. S., Hills, A. J., Blake, N. J., Barth, M. C., Weinheimer, A., Cantrell, C., Rutledge, S. A., Basarab, B., Crawford, J., Diskin, G., Homeyer, C. R., Campos, T., Flocke, F., Fried, A., Blake, D. R., Brune, W., Pollack, I., Peischl, J., Ryerson, T., Wennberg, P. O., Crounse, J. D., Wisthaler, A., Mikoviny, T., Huey, G., Heikes, B., O'Sullivan, D. and Riemer, D. D.: Upper tropospheric ozone production from lightning NO_x-impacted convection: Smoke ingestion case study from the DC3 campaign, J. Geophys. Res Atmos., 120(6), 2505–2523, doi:10.1002/2014jd022121, 2015.

Araizaga, A. E., Mancilla, Y. and Mendoza, A.: Volatile Organic Compound Emissions from Light-Duty Vehicles in Monterrey, Mexico: a Tunnel Study, Int. J. Environ. Res. Public Health, 7(2), 277–292, doi:10.22059/ijer.2013.607, 2013.

Arey, J., Aschmann, S. M., Kwok, E. S. C. and Atkinson, R.: Alkyl Nitrate, Hydroxyalkyl Nitrate, and Hydroxycarbonyl Formation from the NOx−Air Photooxidations of C5−C8 n-Alkanes, J. Phys. Chem. A, 105(6), 1020–1027, doi:10.1021/jp003292z, 2001.

Asher, E., Hornbrook, R. S., Roozitalab, B., Zhang, X., Ortega, J., Tyndall, G. S., Hills, A. J., Orlando, J. J. and Apel, E. C.: Analysis of volatile organic compound product distributions under reduced NO_x conditions in the NSF NCAR atmospheric simulation chamber: Implications for *in situ* VOC measurements, ACS Earth Space Chem., 9(7), 1737–1751, doi:10.1021/acsearthspacechem.4c00407, 2025.

Atkinson, R.: Rate constants for the atmospheric reactions of alkoxy radicals: An updated estimation method, Atmos. Environ., 41(38), 8468–8485, doi:10.1016/j.atmosenv.2007.07.002, 2007.

Atkinson, R. and Arey, J.: Atmospheric degradation of volatile organic compounds, Chem. Rev., 103(12), 4605–4638, doi:10.1021/cr0206420, 2003.

Atkinson, R. and Lloyd, A. C.: Evaluation of kinetic and mechanistic data for modeling of photochemical smog, J. Phys. Chem. Ref. Data, 13(2), 315–444, doi:10.1063/1.555710, 1984.

Atkinson, R., Baulch, D. L., Cox, R. A., Crowley, J. N., Hampson, R. F., Hynes, R. G., Jenkin, M. E., Rossi, M. J. and Troe, J.: Evaluated kinetic and photochemical data for atmospheric chemistry: Volume I - gas phase reactions of O_x, HO_x, NO_x and SO_x species, Atmos. Chem. Phys., 4(6), 1461–1738, doi:10.5194/acp-4-1461-2004, 2004.

https://doi.org/10.5194/egusphere-2026-1868
Preprint. Discussion started: 29 May 2026

Atkinson, R., Baulch, D. L., Cox, R. A., Crowley, J. N., Hampson, R. F., Hynes, R. G., Jenkin, M. E., Rossi, M. J., Troe, J. and IUPAC Subcommittee: Evaluated kinetic and photochemical data for atmospheric chemistry: Volume II – gas phase reactions of organic species, Atmos. Chem. Phys., 6(11), 3625–4055, doi:10.5194/acp-6-3625-2006, 2006.

Aumont, B., Szopa, S. and Madronich, S.: Modelling the evolution of organic carbon during its gas-phase tropospheric oxidation: development of an explicit model based on a self generating approach, Atmos. Chem. Phys., 5(9), 2497–2517, doi:10.5194/acp-5-2497-2005, 2005.

Baker, A. K., Beyersdorf, A. J., Doezema, L. A., Katzenstein, A., Meinardi, S., Simpson, I. J., Blake, D. R. and Sherwood Rowland, F.: Measurements of nonmethane hydrocarbons in 28 United States cities, Atmos. Environ., 42(1), 170–182, doi:10.1016/j.atmosenv.2007.09.007, 2008.

Barnes, I. and Rudzinski, K. J.: Environmental simulation chambers: Application to atmospheric chemical processes, Springer Science & Business Media., 2006.

Bates, K. H. and Jacob, D. J.: A new model mechanism for atmospheric oxidation of isoprene: global effects on oxidants, nitrogen oxides, organic products, and secondary organic aerosol, Atmos. Chem. Phys., 19(14), 9613–9640, doi:10.5194/acp-19-9613-2019, 2019.

Baudic, A., Gros, V., Sauvage, S., Locoge, N., Sanchez, O., Sarda-Estève, R., Kalogridis, C., Petit, J.-E., Bonnaire, N., Baisnée, D., Favez, O., Albinet, A., Sciare, J. and Bonsang, B.: Seasonal variability and source apportionment of volatile organic compounds (VOCs) in the Paris megacity (France), Atmos. Chem. Phys., 16(18), 11961–11989, doi:10.5194/acp-16-11961-2016, 2016.

Bey, I., Jacob, D. J., Yantosca, R. M., Logan, J. A., Field, B. D., Fiore, A. M., Li, Q., Liu, H. Y., Mickley, L. J. and Schultz, M. G.: Global modeling of tropospheric chemistry with assimilated meteorology: Model description and evaluation, J. Geophys. Res., 106(D19), 23073–23095, doi:10.1029/2001jd000807, 2001.

Brasseur, G. P., Hauglustaine, D. A., Walters, S., Rasch, P. J., Müller, J.-F., Granier, C. and Tie, X. X.: MOZART, a global chemical transport model for ozone and related chemical tracers: 1. Model description, J. Geophys. Res., 103(D21), 28265–28289, doi:10.1029/98jd02397, 1998.

Brewer, J. F., Papanastasiou, D. K., Burkholder, J. B., Fischer, E. V., Ren, Y., Mellouki, A. and Ravishankara, A. R.: Atmospheric photolysis of methyl ethyl, diethyl, and propyl ethyl ketones: Temperature-dependent UV absorption cross sections, J. Geophys. Res Atmos., 124(11), 5906–5918, doi:10.1029/2019jd030391, 2019.

Brune, W. H., Miller, D. O. and Thames, A. B.: ATom: Measurements from Airborne Tropospheric Hydrogen Oxides Sensor (ATHOS), V2, , doi:10.3334/ORNLDAAC/1930, 2021.

Burkholder, J. B., Sander, S. P., Abbatt, J., Barker, R., J., Cappa, C., Crounse, J. D., Dibble, T. S., Huie, R. E., Kolb, C. E., Kurylo, M. J., Orkin, V. L., Percival, C. J., Wilmouth, D. M. and and Wine, P. H.: Chemical Kinetics and Photochemical Data for Use in Atmospheric Studies, Evaluation No. 19, JPL Publication 19-5, Jet Propulsion Laboratory. [online] Available from: https://jpldataeval.jpl.nasa.gov, 2019.

Calvert, J., Mellouki, A. and Orlando, J.: The Mechanisms of Atmospheric Oxidation of the Oxygenates, Oxford University Press, USA. [online] Available from: https://play.google.com/store/books/details?id=E22_NbrLuigC, 2011.

Calvert, J. G., Derwent, R. G., Orlando, J. J., Wallington, T. J. and Tyndall, G. S.: Mechanisms of Atmospheric Oxidation of the Alkanes, Oxford University Press, USA. [online] Available from: https://play.google.com/store/books/details?id=uWoSDAAAQBAJ, 2008.

https://doi.org/10.5194/egusphere-2026-1868
Preprint. Discussion started: 29 May 2026

Calvert, J. G., Orlando, J. J., Stockwell, W. R. and Wallington, T. J.: The Mechanisms of Reactions Influencing Atmospheric Ozone, Oxford University Press. [online] Available from: https://play.google.com/store/books/details?id=zATHCQAAQBAJ, 2015.

Carter, W. P. L.: DOCUMENTATION OF THE SAPRC-99 CHEMICAL MECHANISM FOR VOC REACTIVITY ASSESSMENT., 2000.

Chen, Y. and Zhu, L.: The Wavelength Dependence of the Photodissociation of Propionaldehyde in the 280−330 nm Region, J. Phys. Chem. A, 105(42), 9689–9696, doi:10.1021/jp011445s, 2001.

Conner, T. L., Lonneman, W. A. and Seila, R. L.: Transportation-Related Volatile Hydrocarbon Source Profiles Measured in Atlanta, J. Air Waste Manage. Assoc., 45(5), 383–394, doi:10.1080/10473289.1995.10467370, 1995.

Danabasoglu, G., Lamarque, J.-F., Bacmeister, J., Bailey, D. A., DuVivier, A. K., Edwards, J., Emmons, L. K., Fasullo, J., Garcia, R., Gettelman, A., Hannay, C., Holland, M. M., Large, W. G., Lauritzen, P. H., Lawrence, D. M., Lenaerts, J. T. M., Lindsay, K., Lipscomb, W. H., Mills, M. J., Neale, R., Oleson, K. W., Otto-Bliesner, B., Phillips, A. S., Sacks, W., Tilmes, S., Kampenhout, L., Vertenstein, M., Bertini, A., Dennis, J., Deser, C., Fischer, C., Fox-Kemper, B., Kay, J. E., Kinnison, D., Kushner, P. J., Larson, V. E., Long, M. C., Mickelson, S., Moore, J. K., Nienhouse, E., Polvani, L., Rasch, P. J. and Strand, W. G.: The Community Earth System Model Version 2 (CESM2), J. Adv. Model. Earth Syst., 12(2), e2019MS001916, doi:10.1029/2019ms001916, 2020.

Deng, C., Jin, Y., Zhang, M., Liu, X. and Yu, Z.: Emission characteristics of VOCs from on-road vehicles in an urban tunnel in eastern China and predictions for 2017–2026, Aerosol Air Qual. Res., 18(12), 3025–3034, doi:10.4209/aaqr.2018.07.0248, 2018.

Dibble, T. S. and Chai, J.: Critical review of atmospheric chemistry of alkoxy radicals, in Advances in Atmospheric Chemistry, pp. 185–269, World Scientific., 2017.

Dominutti, P., Nogueira, T., Fornaro, A. and Borbon, A.: One decade of VOCs measurements in São Paulo megacity: Composition, variability, and emission evaluation in a biofuel usage context, Sci. Total Environ., 738, 139790, doi:10.1016/j.scitotenv.2020.139790, 2020.

Dominutti, P. A., Nogueira, T., Borbon, A., Andrade, M. de F. and Fornaro, A.: One-year of NMHCs hourly observations in São Paulo megacity: meteorological and traffic emissions effects in a large ethanol burning context, Atmos. Environ., 142, 371–382, doi:10.1016/j.atmosenv.2016.08.008, 2016.

Droege, A. T. and Tully, F. P.: Hydrogen-atom abstraction from alkanes by hydroxyl. 3. Propane, J. Phys. Chem., 90(9), 1949–1954, doi:10.1021/j100400a042, 1986.

Emmons, L. K., Schwantes, R. H., Orlando, J. J., Tyndall, G., Kinnison, D., Lamarque, J.-F., Marsh, D., Mills, M. J., Tilmes, S., Bardeen, C., Buchholz, R. R., Conley, A., Gettelman, A., Garcia, R., Simpson, I., Blake, D. R., Meinardi, S. and Pétron, G.: The Chemistry Mechanism in the Community Earth System Model Version 2 (CESM2), J. Adv. Model. Earth Syst., 12(4), e2019MS001882, doi:10.1029/2019ms001882, 2020.

Ervens, B., Rickard, A., Aumont, B., Carter, W. P. L., McGillen, M., Mellouki, A., Orlando, J., Picquet-Varrault, B., Seakins, P., Stockwell, W. R., Vereecken, L. and Wallington, T. J.: Opinion: Challenges and needs of tropospheric chemical mechanism development, Atmos. Chem. Phys., 24(23), 13317–13339, doi:10.5194/acp-24-13317-2024, 2024.

Flocke, F., Pfister, G., Crawford, J. H., Pickering, K. E., Pierce, G., Bon, D. and Reddy, P.: Air Quality in the northern Colorado Front Range metro area: The Front Range Air Pollution and Photochemistry Éxperiment (FRAPPÉ), J. Geophys. Res Atmos., 125(2), doi:10.1029/2019jd031197, 2020.

https://doi.org/10.5194/egusphere-2026-1868
Preprint. Discussion started: 29 May 2026

Gaubert, B., Emmons, L. K., Raeder, K., Tilmes, S., Miyazaki, K., Arellano, A. F., Jr, Elguindi, N., Granier, C., Tang, W., Barré, J., Worden, H. M., Buchholz, R. R., Edwards, D. P., Franke, P., Anderson, J. L., Saunois, M., Schroeder, J., Woo, J.-H., Simpson, I. J., Blake, D. R., Meinardi, S., Wennberg, P. O., Crounse, J., Teng, A., Kim, M., Dickerson, R. R., He, H., Ren, X., Pusede, S. E. and Diskin, G. S.: Correcting model biases of CO in East Asia: impact on oxidant distributions during KORUS-AQ, Atmos. Chem. Phys., 20(23), 14617–14647, doi:10.5194/acp-20-14617-2020, 2020.

Gelaro, R., McCarty, W., Suárez, M. J., Todling, R., Molod, A., Takacs, L., Randles, C., Darmenov, A., Bosilovich, M. G., Reichle, R., Wargan, K., Coy, L., Cullather, R., Draper, C., Akella, S., Buchard, V., Conaty, A., da Silva, A., Gu, W., Kim, G.-K., Koster, R., Lucchesi, R., Merkova, D., Nielsen, J. E., Partyka, G., Pawson, S., Putman, W., Rienecker, M., Schubert, S. D., Sienkiewicz, M. and Zhao, B.: The modern-Era Retrospective Analysis for Research and Applications, Version 2 (MERRA-2), J. Clim., 30(13), 5419–5454, doi:10.1175/JCLI-D-16-0758.1, 2017.

Gentner, D. R., Worton, D. R., Isaacman, G., Davis, L. C., Dallmann, T. R., Wood, E. C., Herndon, S. C., Goldstein, A. H. and Harley, R. A.: Chemical composition of gas-phase organic carbon emissions from motor vehicles and implications for ozone production, Environ. Sci. Technol., 47(20), 11837–11848, doi:10.1021/es401470e, 2013.

Gilman, J. B., Burkhart, J. F., Lerner, B. M., Williams, E. J., Kuster, W. C., Goldan, P. D., Murphy, P. C., Warneke, C., Fowler, C., Montzka, S. A., Miller, B. R., Miller, L., Oltmans, S. J., Ryerson, T. B., Cooper, O. R., Stohl, A. and de Gouw, J. A.: Ozone variability and halogen oxidation within the Arctic and sub-Arctic springtime boundary layer, Atmos. Chem. Phys., 10(21), 10223–10236, doi:10.5194/acp-10-10223-2010, 2010.

Gilman, J. B., Lerner, B. M., Kuster, W. C. and de Gouw, J. A.: Source signature of volatile organic compounds from oil and natural gas operations in northeastern Colorado, Environ. Sci. Technol., 47(3), 1297–1305, doi:10.1021/es304119a, 2013.

Goldstein, A. H. and Galbally, I. E.: Known and unknown organic constituents in the Earth' s atmosphere, Environ. Sci. Technol., 41(5), 1514–1521, doi:10.1021/es072476p, 2007.

Guenther, A. B., Jiang, X., Heald, C. L., Sakulyanontvittaya, T., Duhl, T., Emmons, L. K. and Wang, X.: The Model of Emissions of Gases and Aerosols from Nature version 2.1 (MEGAN2.1): an extended and updated framework for modeling biogenic emissions, Geosci. Model Dev., 5(6), 1471–1492, doi:10.5194/gmd-5-1471-2012, 2012.

Hecobian, A., Clements, A. L., Shonkwiler, K. B., Zhou, Y., MacDonald, L. P., Hilliard, N., Wells, B. L., Bibeau, B., Ham, J. M., Pierce, J. R. and Collett, J. L., Jr: Air Toxics and Other Volatile Organic Compound Emissions from Unconventional Oil and Gas Development, Environ. Sci. Technol. Lett., 6(12), 720–726, doi:10.1021/acs.estlett.9b00591, 2019.

Heicklen, J., Desai, J., Bahta, A., Harper, C. and Simonaitis, R.: The temperature and wavelength dependence of the photo-oxidation of propionaldehyde, J. Photochem., 34(2), 117–135, doi:10.1016/0047-2670(86)85014-6, 1986.

Herrington, A. R., Lauritzen, P. H., Taylor, M. A., Goldhaber, S., Eaton, B. E., Bacmeister, J. T., Reed, K. A. and Ullrich, P. A.: Physics–dynamics coupling with element-based high-order Galerkin methods: Quasi-equal-area physics grid, Mon. Weather Rev., 147(1), 69–84, doi:10.1175/mwr-d-18-0136.1, 2019.

Ho, K. F., Lee, S. C., Ho, W. K., Blake, D. R., Cheng, Y., Li, Y. S., Ho, S. S. H., Fung, K., Louie, P. K. K. and Park, D.: Vehicular emission of volatile organic compounds (VOCs) from a tunnel study in Hong Kong, Atmos. Chem. Phys., 9(19), 7491–7504, doi:10.5194/acp-9-7491-2009, 2009.

Horowitz, A. and Calvert, J. G.: Wavelength dependence of the primary processes in acetaldehyde photolysis, J. Phys. Chem., 86(16), 3105–3114, doi:10.1021/j100213a011, 1982.

Huang, L., Jiang, J. H., Murray, L. T., Damon, M. R., Su, H. and Livesey, N. J.: Evaluation of UTLS carbon monoxide simulations in GMI and GEOS-Chem chemical transport models using Aura MLS observations, Atmos. Chem. Phys., 16(9), 5641–5663, doi:10.5194/acp-16-5641-2016, 2016.

https://doi.org/10.5194/egusphere-2026-1868
Preprint. Discussion started: 29 May 2026

Hwa, M.-Y., Hsieh, C.-C., Wu, T.-C. and Chang, L.-F. W.: Real-world vehicle emissions and VOCs profile in the Taipei tunnel located at Taiwan Taipei area, Atmos. Environ., 36(12), 1993–2002, doi:10.1016/S1352-2310(02)00148-6, 2002.

Jenkin, M. E., Saunders, S. M. and Pilling, M. J.: The tropospheric degradation of volatile organic compounds: a protocol for mechanism development, Atmos. Environ., 31(1), 81–104, doi:10.1016/S1352-2310(96)00105-7, 1997.

Jenkin, M. E., Young, J. C. and Rickard, A. R.: The MCM v3.3.1 degradation scheme for isoprene, Atmos. Chem. Phys., 15(20), 11433–11459, doi:10.5194/acp-15-11433-2015, 2015.

Jenkin, M. E., Valorso, R., Aumont, B., Rickard, A. R. and Wallington, T. J.: Estimation of rate coefficients and branching ratios for gas-phase reactions of OH with aliphatic organic compounds for use in automated mechanism construction, Atmos. Chem. Phys., 18(13), 9297–9328, doi:10.5194/acp-18-9297-2018, 2018.

Jenkin, M. E., Valorso, R., Aumont, B. and Rickard, A. R.: Estimation of rate coefficients and branching ratios for reactions of organic peroxy radicals for use in automated mechanism construction, Atmos. Chem. Phys., 19(11), 7691–7717, doi:10.5194/acp-19-7691-2019, 2019.

Jo, D. S., Hodzic, A., Emmons, L. K., Tilmes, S., Schwantes, R. H., Mills, M. J., Campuzano-Jost, P., Hu, W., Zaveri, R. A., Easter, R. C., Singh, B., Lu, Z., Schulz, C., Schneider, J., Shilling, J. E., Wisthaler, A. and Jimenez, J. L.: Future changes in isoprene-epoxydiol-derived secondary organic aerosol (IEPOX SOA) under the Shared Socioeconomic Pathways: the importance of physicochemical dependency, Atmos. Chem. Phys., 21(5), 3395–3425, doi:10.5194/acp-21-3395-2021, 2021.

Jo, D. S., Tilmes, S., Emmons, L. K., Wang, S. and Vitt, F.: A new simplified parameterization of secondary organic aerosol in the Community Earth System Model Version 2 (CESM2; CAM6.3), Geosci. Model Dev., 16(13), 3893–3906, doi:10.5194/gmd-16-3893-2023, 2023a.

Jo, D. S., Emmons, L. K., Callaghan, P., Tilmes, S., Woo, J.-H., Kim, Y., Kim, J., Granier, C., Soulié, A., Doumbia, T., Darras, S., Buchholz, R. R., Simpson, I. J., Blake, D. R., Wisthaler, A., Schroeder, J. R., Fried, A. and Kanaya, Y.: Comparison of urban air quality simulations during the KORUS-AQ campaign with regionally refined versus global uniform grids in the Multi-Scale Infrastructure for Chemistry and Aerosols (MUSICA) version 0, J. Adv. Model. Earth Syst., 15(7), e2022MS003458, doi:10.1029/2022ms003458, 2023b.

Kaduwela, A., Luecken, D., Carter, W. and Derwent, R.: New directions: Atmospheric chemical mechanisms for the future, Atmos. Environ., 122, 609–610, doi:10.1016/j.atmosenv.2015.10.031, 2015.

Kim, H., Park, R. J., Kim, S., Brune, W. H., Diskin, G. S., Fried, A., Hall, S. R., Weinheimer, A. J., Wennberg, P., Wisthaler, A. and Others: Observed versus simulated OH reactivity during KORUS-AQ campaign: Implications for emission inventory and chemical environment in East Asia, Elem Sci Anth, 10(1), 00030, doi:10.1525/elementa.2022.00030, 2022.

Kinnison, D. E., Brasseur, G. P., Walters, S., Garcia, R. R., Marsh, D. R., Sassi, F., Harvey, V. L., Randall, C. E., Emmons, L., Lamarque, J. F., Hess, P., Orlando, J. J., Tie, X. X., Randel, W., Pan, L. L., Gettelman, A., Granier, C., Diehl, T., Niemeier, U. and Simmons, A. J.: Sensitivity of chemical tracers to meteorological parameters in the MOZART-3 chemical transport model, J. Geophys. Res., 112(D20), doi:10.1029/2006jd007879, 2007.

Lanz, V. A., Hueglin, C., Buchmann, B., Hill, M., Locher, R., Staehelin, J. and Reimann, S.: Receptor modeling of C_2–C_7 hydrocarbon sources at an urban background site in Zurich, Switzerland: changes between 1993–1994 and 2005–2006, Atmos. Chem. Phys., 8(9), 2313–2332, doi:10.5194/acp-8-2313-2008, 2008.

Lauritzen, P.: CAM7 development update, [online] Available from: https://www.cesm.ucar.edu/sites/default/files/2025-06/2025cesmlauritzen.pdf, 2025.

https://doi.org/10.5194/egusphere-2026-1868
Preprint. Discussion started: 29 May 2026

Lauritzen, P. H., Nair, R. D., Herrington, A. R., Callaghan, P., Goldhaber, S., Dennis, J. M., Bacmeister, J. T., Eaton, B. E., Zarzycki, C. M., Taylor, M. A., Ullrich, P. A., Dubos, T., Gettelman, A., Neale, R. B., Dobbins, B., Reed, K. A., Hannay, C., Medeiros, B., Benedict, J. J. and Tribbia, J. J.: NCAR Release of CAM-SE in CESM2.0: A Reformulation of the Spectral Element Dynamical Core in Dry-Mass Vertical Coordinates With Comprehensive Treatment of Condensates and Energy, J. Adv. Model. Earth Syst., 10(7), 1537–1570, doi:10.1029/2017MS001257, 2018.

Lawrence, P. J. and Chase, T. N.: Representing a new MODIS consistent land surface in the Community Land Model (CLM 3.0), J. Geophys. Res., 112(G1), doi:10.1029/2006jg000168, 2007.

Lin, H., Emmons, L. K., Lundgren, E. W., Yang, L. H., Feng, X., Dang, R., Zhai, S., Tang, Y., Kelp, M. M., Colombi, N. K., Eastham, S. D., Fritz, T. M. and Jacob, D. J.: Intercomparison of GEOS-Chem and CAM-chem tropospheric oxidant chemistry within the Community Earth System Model version 2 (CESM2), Atmos. Chem. Phys., 24(15), 8607–8624, doi:10.5194/acp-24-8607-2024, 2024.

Madronich, S. and Flocke, S.: The role of solar radiation in atmospheric chemistry, in The Handbook of Environmental Chemistry, pp. 1–26, Springer Berlin Heidelberg, Berlin, Heidelberg., 1999.

Martins, L. D., Andrade, M. F., Freitas, E. D., Pretto, A., Gatti, L. V., Albuquerque, E. L., Tomaz, E., Guardani, M. L., Martins, M. H. R. B. and Junior, O. M. A.: Emission factors for gas-powered vehicles traveling through road tunnels in São Paulo, Brazil, Environ. Sci. Technol., 40(21), 6722–6729, doi:10.1021/es052441u, 2006.

McDuffie, E. E., Fibiger, D. L., Dubé, W. P., Lopez-Hilfiker, F., Lee, B. H., Thornton, J. A., Shah, V., Jaeglé, L., Guo, H., Weber, R. J., Michael Reeves, J., Weinheimer, A. J., Schroder, J. C., Campuzano-Jost, P., Jimenez, J. L., Dibb, J. E., Veres, P., Ebben, C., Sparks, T. L., Wooldridge, P. J., Cohen, R. C., Hornbrook, R. S., Apel, E. C., Campos, T., Hall, S. R., Ullmann, K. and Brown, S. S.: Heterogeneous N_2O_5 uptake during winter: Aircraft measurements during the 2015 WINTER campaign and critical evaluation of current parameterizations, J. Geophys. Res Atmos., 123(8), 4345–4372, doi:10.1002/2018jd028336, 2018.

McDuffie, E. E., Smith, S. J., O'Rourke, P., Tibrewal, K., Venkataraman, C., Marais, E. A., Zheng, B., Crippa, M., Brauer, M. and Martin, R. V.: A global anthropogenic emission inventory of atmospheric pollutants from sector- and fuel-specific sources (1970–2017): an application of the Community Emissions Data System (CEDS), Earth Syst. Sci. Data, 12(4), 3413–3442, doi:10.5194/essd-12-3413-2020, 2020.

McKain, K. and Sweeney, C.: ATom: CO2, CH4, and CO Measurements from Picarro, 2016-2018, , doi:10.3334/ORNLDAAC/1732, 2021.

Mouchel-Vallon, C., Lee-Taylor, J., Hodzic, A., Artaxo, P., Aumont, B., Camredon, M., Gurarie, D., Jimenez, J.-L., Lenschow, D. H., Martin, S. T., Nascimento, J., Orlando, J. J., Palm, B. B., Shilling, J. E., Shrivastava, M. and Madronich, S.: Exploration of oxidative chemistry and secondary organic aerosol formation in the Amazon during the wet season: explicit modeling of the Manaus urban plume with GECKO-A, Atmos. Chem. Phys., 20(10), 5995–6014, doi:10.5194/acp-20-5995-2020, 2020.

Orlando, J. J. and Tyndall, G. S.: Laboratory studies of organic peroxy radical chemistry: an overview with emphasis on recent issues of atmospheric significance, Chem. Soc. Rev., 41(19), 6294–6317, doi:10.1039/c2cs35166h, 2012.

Orlando, J. J., Tyndall, G. S. and Wallington, T. J.: The atmospheric chemistry of alkoxy radicals, Chem. Rev., 103(12), 4657–4690, doi:10.1021/cr020527p, 2003.

Pan, L. L., E. L. Atlas, Newman, P. A., Thornberry, T., Jucks, K. W., Toon, O. B., Randel, W. J., Liang, Q., Kinnison, D. E., Ueyama, R., Bresch, J. F., Honomichl, S. B., Smith, W. P., Hornbrook, R. S., Ziemba, L., Fujiwara, M., Apel, E. C., Barucci, M., Bianchini, G., Brown, M., Bui, T. P., Campos, T., Chin, M., D'Amato, F., Dean-Day, J., Diskin, G., Franchin, A., Gurganus, C., Iraci, L. T., Kim, J., Koo, J.-H., Lait, L. R., Lesko, K., Podolske, J. R., Rollins, A., Sakai, T., Shiraishi, K., Treadaway, V.,

https://doi.org/10.5194/egusphere-2026-1868
Preprint. Discussion started: 29 May 2026

Viciani, S. and Waxman, E.: The Asian Summer Monsoon chemical and Climate Impact Project (ACCLIP): An overview, J. Geophys. Res Atmos., 130(23), doi:10.1029/2025jd044417, 2025.

Pang, Y., Fuentes, M. and Rieger, P.: Trends in the emissions of Volatile Organic Compounds (VOCs) from light-duty gasoline vehicles tested on chassis dynamometers in Southern California, Atmos. Environ., 83, 127–135, doi:10.1016/j.atmosenv.2013.11.002, 2014.

Pfister, G. G., Eastham, S. D., Arellano, A. F., Aumont, B., Barsanti, K. C., Barth, M. C., Conley, A., Davis, N. A., Emmons, L. K., Fast, J. D., Fiore, A. M., Gaubert, B., Goldhaber, S., Granier, C., Grell, G. A., Guevara, M., Henze, D. K., Hodzic, A., Liu, X., Marsh, D. R., Orlando, J. J., Plane, J. M. C., Polvani, L. M., Rosenlof, K. H., Steiner, A. L., Jacob, D. J. and Brasseur, G. P.: The Multi-Scale Infrastructure for Chemistry and Aerosols (MUSICA), Bull. Am. Meteorol. Soc., 101(10), E1743–E1760, doi:10.1175/BAMS-D-19-0331.1, 2020.

Pinho, P. G., Pio, C. A. and Jenkin, M. E.: Evaluation of isoprene degradation in the detailed tropospheric chemical mechanism, MCM v3, using environmental chamber data, Atmos. Environ., 39(7), 1303–1322, doi:10.1016/j.atmosenv.2004.11.014, 2005.

Praske, E., Otkjær, R. V., Crounse, J. D., Hethcox, J. C., Stoltz, B. M., Kjaergaard, H. G. and Wennberg, P. O.: Atmospheric autoxidation is increasingly important in urban and suburban North America, Proc. Natl. Acad. Sci. U. S. A., 115(1), 64–69, doi:10.1073/pnas.1715540115, 2018.

Pye, H. O. T., Place, B. K., Murphy, B. N., Seltzer, K. M., D'Ambro, E. L., Allen, C., Piletic, I. R., Farrell, S., Schwantes, R. H., Coggon, M. M., Saunders, E., Xu, L., Sarwar, G., Hutzell, W. T., Foley, K. M., Pouliot, G., Bash, J. and Stockwell, W. R.: Linking gas, particulate, and toxic endpoints to air emissions in the Community Regional Atmospheric Chemistry Multiphase Mechanism (CRACMM), Atmos. Chem. Phys., 23(9), 5043–5099, doi:10.5194/acp-23-5043-2023, 2023.

Raber, W. H. and Moortgat, G. K.: PHOTOOXIDATION OF SELECTED CARBONYL COMPOUNDS IN AIR: METHYL ETHYL KETONE, METHYL VINYL KETONE, METHACROLEIN AND METHYLGLYOXAL, in Progress and Problems in Atmospheric Chemistry, p. Chap. 9, WORLD SCIENTIFIC., 1987.

Raventos-Duran, T., Camredon, M., Valorso, R., Mouchel-Vallon, C. and Aumont, B.: Structure-activity relationships to estimate the effective Henry's law constants of organics of atmospheric interest, Atmos. Chem. Phys., 10(16), 7643–7654, doi:10.5194/acp-10-7643-2010, 2010.

Roehl, C. M., Bauer, D. and Moortgat, G. K.: Absorption Spectrum and Kinetics of the Acetylperoxy Radical, J. Phys. Chem., 100(10), 4038–4047, doi:10.1021/jp9526298, 1996.

Romero, M. T. B., Blitz, M. A., Heard, D. E., Pilling, M. J., Price, B., Seakins, P. W. and Wang, L.: Photolysis of methylethyl, diethyl and methylvinyl ketones and their role in the atmospheric HOx budget, Faraday Discuss., 130, 73–88; discussion 125-51, 519–24, doi:10.1039/b419160a, 2005.

Rossabi, S. and Helmig, D.: Changes in atmospheric butanes and pentanes and their isomeric ratios in the continental United States, J. Geophys. Res Atmos., 123(7), 3772–3790, doi:10.1002/2017jd027709, 2018.

Ryerson, T. B., Thompson, C. R., Peischl, J. and Bourgeois, I.: ATom: L2 in situ measurements from NOAA Nitrogen Oxides and ozone (NOyO3) instrument, , doi:10.3334/ORNLDAAC/1734, 2019.

Sander, R.: Compilation of Henry's law constants (version 4.0) for water as solvent, Atmos. Chem. Phys., 15(8), 4399–4981, doi:10.5194/acp-15-4399-2015, 2015.

Santos, E. M. and Azevedo, D. de A.: Impact on ground-level ozone formation by emission characterization of volatile organic compounds from a flex-fuel light-duty vehicle fleet in a traffic tunnel in Rio de Janeiro, Brazil, Air Qual. Atmos. Health, 14(2), 259–270, doi:10.1007/s11869-020-00931-6, 2021.

https://doi.org/10.5194/egusphere-2026-1868
Preprint. Discussion started: 29 May 2026

Saunders, S. M., Jenkin, M. E., Derwent, R. G. and Pilling, M. J.: Protocol for the development of the Master Chemical Mechanism, MCM v3 (Part A): tropospheric degradation of non-aromatic volatile organic compounds, Atmos. Chem. Phys., 3(1), 161–180, doi:10.5194/acp-3-161-2003, 2003.

Schwantes, R. H., Emmons, L. K., Orlando, J. J., Barth, M. C., Tyndall, G. S., Hall, S. R., Ullmann, K., Clair, J. M. S., Blake, D. R., Wisthaler, A. and Bui, T. P. V.: Comprehensive isoprene and terpene gas-phase chemistry improves simulated surface ozone in the southeastern US, Atmos. Chem. Phys., 20(6), 3739–3776, doi:10.5194/acp-20-3739-2020, 2020.

Schwantes, R. H., Lacey, F. G., Tilmes, S., Emmons, L. K., Lauritzen, P. H., Walters, S., Callaghan, P., Zarzycki, C. M., Barth, M. C., Jo, D. S., Bacmeister, J. T., Neale, R. B., Vitt, F., Kluzek, E., Roozitalab, B., Hall, S. R., Ullmann, K., Warneke, C., Peischl, J., Pollack, I. B., Flocke, F., Wolfe, G. M., Hanisco, T. F., Keutsch, F. N., Kaiser, J., Bui, T. P. V., Jimenez, J. L., Campuzano-Jost, P., Apel, E. C., Hornbrook, R. S., Hills, A. J., Yuan, B. and Wisthaler, A.: Evaluating the impact of chemical complexity and horizontal resolution on tropospheric ozone over the conterminous US with a global variable resolution chemistry model, J. Adv. Model. Earth Syst., 14(6), e2021MS002889, doi:10.1029/2021ms002889, 2022.

Simpson, I. J., Blake, N. J., Barletta, B., Diskin, G. S., Fuelberg, H. E., Gorham, K., Huey, L. G., Meinardi, S., Rowland, F. S., Vay, S. A., Weinheimer, A. J., Yang, M. and Blake, D. R.: Characterization of trace gases measured over Alberta oil sands mining operations: 76 speciated C_2–C_{10} volatile organic compounds (VOCs), CO_2, CH_4, CO, NO, NO_2, NO_y, O_3 and SO_2, Atmos. Chem. Phys., 10(23), 11931–11954, doi:10.5194/acp-10-11931-2010, 2010.

Simpson, I. J., Aburizaiza, O. S., Siddique, A., Barletta, B., Blake, N. J., Gartner, A., Khwaja, H., Meinardi, S., Zeb, J. and Blake, D. R.: Air quality in Mecca and surrounding holy places in Saudi Arabia during Hajj: initial survey, Environ. Sci. Technol., 48(15), 8529–8537, doi:10.1021/es5017476, 2014.

Simpson, I. J., Blake, D. R., Blake, N. J., Meinardi, S., Barletta, B., Hughes, S. C., Fleming, L. T., Crawford, J. H., Diskin, G. S., Emmons, L. K., Fried, A., Guo, H., Peterson, D. A., Wisthaler, A., Woo, J.-H., Barré, J., Gaubert, B., Kim, J., Kim, M. J., Kim, Y., Knote, C., Mikoviny, T., Pusede, S. E., Schroeder, J. R., Wang, Y., Wennberg, P. O. and Zeng, L.: Characterization, sources and reactivity of volatile organic compounds (VOCs) in Seoul and surrounding regions during KORUS-AQ, Elem. Sci. Anth., 8(1), 37, doi:10.1525/elementa.434, 2020.

Song, C., Liu, Y., Sun, L., Zhang, Q. and Mao, H.: Emissions of volatile organic compounds (VOCs) from gasoline- and liquified natural gas (LNG)-fueled vehicles in tunnel studies, Atmos. Environ., 234, 117626, doi:10.1016/j.atmosenv.2020.117626, 2020.

Soulie, A., Granier, C., Darras, S., Zilbermann, N., Doumbia, T., Guevara, M., Jalkanen, J.-P., Keita, S., Liousse, C., Crippa, M., Guizzardi, D., Hoesly, R. and Smith, S. J.: Global anthropogenic emissions (CAMS-GLOB-ANT) for the Copernicus Atmosphere Monitoring Service simulations of air quality forecasts and reanalyses, Earth Syst. Sci. Data, 16(5), 2261–2279, doi:10.5194/essd-16-2261-2024, 2024.

Stein, O., Schultz, M. G., Bouarar, I., Clark, H., Huijnen, V., Gaudel, A., George, M. and Clerbaux, C.: On the wintertime low bias of Northern Hemisphere carbon monoxide found in global model simulations, Atmos. Chem. Phys., 14(17), 9295–9316, doi:10.5194/acp-14-9295-2014, 2014.

Stemmler, K., Bugmann, S., Buchmann, B., Reimann, S. and Staehelin, J.: Large decrease of VOC emissions of Switzerland's car fleet during the past decade: results from a highway tunnel study, Atmos. Environ., 39(6), 1009–1018, doi:10.1016/j.atmosenv.2004.10.010, 2005.

Swarthout, R. F., Russo, R. S., Zhou, Y., Hart, A. H. and Sive, B. C.: Volatile organic compound distributions during the NACHTT campaign at the Boulder Atmospheric Observatory: Influence of urban and natural gas sources, J. Geophys. Res Atmos., 118(18), 10,614-10,637, doi:10.1002/jgrd.50722, 2013.

https://doi.org/10.5194/egusphere-2026-1868
Preprint. Discussion started: 29 May 2026

Swarthout, R. F., Russo, R. S., Zhou, Y., Miller, B. M., Mitchell, B., Horsman, E., Lipsky, E., McCabe, D. C., Baum, E. and Sive, B. C.: Impact of Marcellus Shale natural gas development in southwest Pennsylvania on volatile organic compound emissions and regional air quality, Environ. Sci. Technol., 49(5), 3175–3184, doi:10.1021/es504315f, 2015.

Tang, W., Emmons, L. K., Wiedinmyer, C., Partha, D. B., Huang, Y., He, C., Zhang, J., Barsanti, K. C., Gaubert, B., Jo, D. S., Zhang, J., Buchholz, R., Tilmes, S., Vitt, F., Granier, C., Worden, H. M. and Levelt, P. F.: Disproportionately large impacts of wildland-urban interface fire emissions on global air quality and human health, Sci. Adv., 11(11), doi:10.1126/sciadv.adr2616, 2025.

Thompson, C. R., Wofsy, S. C., Prather, M. J., Newman, P. A., Hanisco, T. F., Ryerson, T. B., Fahey, D. W., Apel, E. C., Brock, C. A., Brune, W. H., Froyd, K., Katich, J. M., Nicely, J. M., Peischl, J., Ray, E., Veres, P. R., Wang, S., Allen, H. M., Asher, E., Bian, H., Blake, D., Bourgeois, I., Budney, J., Paul Bui, T., Butler, A., Campuzano-Jost, P., Chang, C., Chin, M., Commane, R., Correa, G., Crounse, J. D., Daube, B., Dibb, J. E., DiGangi, J. P., Diskin, G. S., Dollner, M., Elkins, J. W., Fiore, A. M., Flynn, C. M., Guo, H., Hall, S. R., Hannun, R. A., Hills, A., Hintsa, E. J., Hodzic, A., Hornbrook, R. S., Greg Huey, L., Jimenez, J. L., Keeling, R. F., Kim, M. J., Kupc, A., Lacey, F., Lait, L. R., Lamarque, J.-F., Liu, J., McKain, K., Meinardi, S., Miller, D. O., Montzka, S. A., Moore, F. L., Morgan, E. J., Murphy, D. M., Murray, L. T., Nault, B. A., Andrew Neuman, J., Nguyen, L., Gonzalez, Y., Rollins, A., Rosenlof, K., Sargent, M., Schill, G., Schwarz, J. P., St. Clair, J. M., Steenrod, S. D., Stephens, B. B., Strahan, S. E., Strode, S. A., Sweeney, C., Thames, A. B., Ullmann, K., Wagner, N., Weber, R., Weinzierl, B., Wennberg, P. O., Williamson, C. J., Wolfe, G. M. and Zeng, L.: The NASA Atmospheric Tomography (ATom) Mission: Imaging the Chemistry of the Global Atmosphere, Bull. Am. Meteorol. Soc., 103(3), E761–E790, doi:10.1175/BAMS-D-20-0315.1, 2022.

Travis, K. R., Nault, B. A., Crawford, J. H., Bates, K. H., Blake, D. R., Cohen, R. C., Fried, A., Hall, S. R., Huey, L. G., Lee, Y. R., Meinardi, S., Min, K.-E., Simpson, I. J. and Ullman, K.: Impact of improved representation of volatile organic compound emissions and production of NO_x reservoirs on modeled urban ozone production, Atmos. Chem. Phys., 24(16), 9555–9572, doi:10.5194/acp-24-9555-2024, 2024.

Tzompa-Sosa, Z. A., Henderson, B. H., Keller, C. A., Travis, K., Mahieu, E., Franco, B., Estes, M., Helmig, D., Fried, A., Richter, D., Weibring, P., Walega, J., Blake, D. R., Hannigan, J. W., Ortega, I., Conway, S., Strong, K. and Fischer, E. V.: Atmospheric implications of large C2-C5 alkane emissions from the U.S. oil and gas industry, J. Geophys. Res Atmos., 124(2), 1148–1169, doi:10.1029/2018JD028955, 2019.

Vereecken, L. and Nozière, B.: H migration in peroxy radicals under atmospheric conditions, Atmos. Chem. Phys., 20(12), 7429–7458, doi:10.5194/acp-20-7429-2020, 2020.

Vereecken, L. and Peeters, J.: Decomposition of substituted alkoxy radicals--part I: a generalized structure-activity relationship for reaction barrier heights, Phys. Chem. Chem. Phys., 11(40), 9062–9074, doi:10.1039/b909712k, 2009.

Wang, S., Hornbrook, R. S., Hills, A., Emmons, L. K., Tilmes, S., Lamarque, J., Jimenez, J. L., Campuzano-Jost, P., Nault, B. A., Crounse, J. D., Wennberg, P. O., Kim, M., Allen, H., Ryerson, T. B., Thompson, C. R., Peischl, J., Moore, F., Nance, D., Hall, B., Elkins, J., Tanner, D., Huey, L. G., Hall, S. R., Ullmann, K., Orlando, J. J., Tyndall, G. S., Flocke, F. M., Ray, E., Hanisco, T. F., Wolfe, G. M., St. Clair, J., Commane, R., Daube, B., Barletta, B., Blake, D. R., Weinzierl, B., Dollner, M., Conley, A., Vitt, F., Wofsy, S. C., Riemer, D. D. and Apel, E. C.: Atmospheric Acetaldehyde: Importance of Air-Sea Exchange and a Missing Source in the Remote Troposphere, Geophys. Res. Lett., 46(10), 5601–5613, doi:10.1029/2019GL082034, 2019.

Wennberg, P. O., Bates, K. H., Crounse, J. D., Dodson, L. G., McVay, R. C., Mertens, L. A., Nguyen, T. B., Praske, E., Schwantes, R. H., Smarte, M. D., St Clair, J. M., Teng, A. P., Zhang, X. and Seinfeld, J. H.: Gas-Phase Reactions of Isoprene and Its Major Oxidation Products, Chem. Rev., 118(7), 3337–3390, doi:10.1021/acs.chemrev.7b00439, 2018.

Wiedinmyer, C., Kimura, Y., McDonald-Buller, E. C., Emmons, L. K., Buchholz, R. R., Tang, W., Seto, K., Joseph, M. B., Barsanti, K. C., Carlton, A. G. and Yokelson, R.: The Fire Inventory from NCAR version 2.5: an updated global fire emissions model for climate and chemistry applications, Geosci. Model Dev., 16(13), 3873–3891, doi:10.5194/gmd-16-3873-2023, 2023.

https://doi.org/10.5194/egusphere-2026-1868
Preprint. Discussion started: 29 May 2026

Wilde, S. E., Dominutti, P. A., Allen, G., Andrews, S. J., Bateson, P., Bauguitte, S. J.-B., Burton, R. R., Colfescu, I., France, J., Hopkins, J. R., Huang, L., Jones, A. E., Lachlan-Cope, T., Lee, J. D., Lewis, A. C., Mobbs, S. D., Weiss, A., Young, S. and Purvis, R. M.: Speciation of VOC emissions related to offshore North Sea oil and gas production, Atmos. Chem. Phys., 21(5), 3741–3762, doi:10.5194/acp-21-3741-2021, 2021.

995 Zhang, Y., Yang, W., Simpson, I., Huang, X., Yu, J., Huang, Z., Wang, Z., Zhang, Z., Liu, D., Huang, Z., Wang, Y., Pei, C., Shao, M., Blake, D. R., Zheng, J., Huang, Z. and Wang, X.: Decadal changes in emissions of volatile organic compounds (VOCs) from on-road vehicles with intensified automobile pollution control: Case study in a busy urban tunnel in south China, Environ. Pollut., 233, 806–819, doi:10.1016/j.envpol.2017.10.133, 2018.